SELENIUM NANOPARTICLES PREPARED BY MYCO-FABRICATION: A NOVEL BONE-FORMING AGENT FOR MANAGING/PREVENTING POSTMENOPAUSAL OSTEOPOROSIS

LUK KAR HIM

Ph.D

The Hong Kong Polytechnic University

2017

The Hong Kong Polytechnic University

Department of Applied Biology and Chemical Technology

Selenium Nanoparticles Prepared by Myco-fabrication: A Novel Bone-forming Agent for Managing/Preventing Postmenopausal Osteoporosis

LUK KAR HIM

A thesis submitted in partial fulfillment of the requirements for the degree of Doctor of Philosophy

August 2016

CERTIFICATION OF ORIGINALITY

I hereby declare that this thesis is my own work and that, to the best of my knowledge and belief, it reproduces no material previously published or written nor material which has been accepted for the award of any other degree or diploma, except where due acknowledgement has been made in the text.

(Signature)

LUK KAR HIM, PETER (Name of Student)

31/08/2017(Date)

ABSTRACT

Osteoporosis is a skeletal disease characterized by low bone mass and density as well as deterioration in bone microarchitecture, leading to high risk of bone fracture. With an increase in aging population, osteoporosis has become one of the major public health issues nowadays, causing significant medical and socioeconomic burdens.

Selenium is an essential trace mineral to human health. Substantial evidences have demonstrated that selenium deficiency is detrimental to bone microarchitecture and even associated with osteopenia, Kashin-Beck osteoarthropathy and osteoporosis, suggesting its crucial role in bone metabolism. Recently, selenium nanoparticles (SeNPs) have become the new research target, since they were found to possess relatively low toxicity and remarkable anti-tumor efficacy compared to other organic and inorganic selenocompounds. Nevertheless, scientific research concerning their effects on bone health is currently very limited.

By using the mushroom polysaccharide-protein complex (PSP) isolated from *Pleurotus tuber-regium*, our research team has successfully prepared novel SeNPs (PTR-SeNPs) under a simple redox system [US patent no.: 9,072,669]. We

discovered that PTR-SeNPs existed as well-dispensed spherical particles in water with an average diameter of 91.3 ± 1.53 nm and was highly stable without significant increase in size after 13 weeks. Further characterization using TEM also showed that the particle size of SeNPs in PTR-SeNPs was around 20 nm. For individual SeNP, the clear lattice fringes (3.34Å), SAED pattern as well as EDX spectrum obtained by HR-TEM-EDX collectively indicated that the resulting nanoparticle possessed a polycrystalline structure with high level of Se (81.2%), implying a successfully fabrication of SeNPs using mushroom PSP.

Endocytosis has been widely reported as the major cellular uptake mechanism for nanoparticles. Our study found that coumarin-6 labelled PTR-SeNPs mainly localized in lysosomes of the murine preosteoblast MC3T3-E1 subclone 4 cells (bone forming progenitor cells) as early as 5 min after cellular internalization. It is the first study of its kind to report the intracellular localization of SeNPs by MC3T3-E1 cells via endocytosis. Besides, substantial previous findings have demonstrated that promoting bone formation is one of the effective strategies to prevent and/or manage postmenopausal osteoporosis. Interestingly, our study indicated that PTR-SeNPs was found to exhibit a significant dose-dependent proliferation effect (range from 1.33 – 1.73 folds) on the MC3T3-E1 cells for 24, 48

and 72 hours with the most effect dosage of 10μM. More importantly, PTR-SeNPs (10μM) were found to markedly induce both osteoblast differentiation and bone mineral formation of the MC3T3-E1 cells as evidenced by a significant increase in ALP activity (1.36 ± 0.10 folds), as well as an enhancement of bone nodule formation (Von Kossa and Alizarin Red S staining). Further investigation on their possible interaction with osteoclasts (bone resorption cells) also showed that PTR-SeNPs could significantly up-regulate the gene expression ratio of the bone remodeling markers OPG/RANKL (2.11 ± 0.33 folds), suggesting their indirect inhibition effect on osteoclastogenesis in addition to promoting osteoblastogenesis.

Osteoblast differentiation is a crucial step of bone formation. Previous studies have demonstrated that BMP-2 signaling via Smad-dependent and/or Smad-independent pathway(s) is one of the most important signaling transduction cascades for regulating osteoblast differentiation. Interestingly, our study discovered that PTR-SeNPs could trigger both BMP-2/Smad dependent and independent pathways simultaneously as evidenced by a significant upregulation of BMP-2 gene expression (1.64 ± 0.24 folds) as well as Smad 1/5/8 (1.31 ± 0.15 folds), ERK (3.67 ± 1.48 folds), p38 (2.86 ± 0.58 folds) and JNK (1.36 ± 0.07 folds) proteins phosphorylation in the MC3T3-E1 cells after 4-day treatment. Besides, PTR-SeNPs

were found to significantly up-regulate the gene expression of those major downstream biomarkers in bone remodeling such as Dlx5 (1.54 ± 0.06 folds), Runx2 (2.11 ± 0.1 folds), Osx (1.87 ± 0.60 folds), ALP (2.09 ± 0.10 folds), and OCN (9.69 ± 1.07 folds), further supporting their active role in promotion of osteoblast differentiation and bone mineralization.

Last but not least, by using *Oryzias latipes* (medaka) larvae, we have successfully established a brand new *in vivo* model to investigate the simulating effect of PTR-SeNPs on bone formation. And we found that PTR-SeNPs (10ppm) could significantly enhance the vertebrate development (both bone and cartilage) of medaka larvae after feeding for 11 days as visualized by Alizarin Red S and Alcian Blue double staining. Consistent with the findings of *in vitro* study, the gene expression level of those major osteogenic markers such as ALP (1.53 ± 0.1 folds), Runx2 (1.45 ± 0.10 folds), Osx (1.41 ± 0.15 folds) as well as OPG/RANKL (4.38 ± 1.31 folds) were all significantly upregulated. Findings of this study could provide significant insights into the *in vitro* and *in vivo* effects of PTR-SeNPs on bone formation. Besides, medaka larvae, as a novel non-mammalian animal model for bone formation study, could be further developed into a rapid and economical *in vivo* screening platform for bone formation prior to conducting traditional animal study

using mice or rats. Our long-term goal is to develop an evidence-based bone-forming agent for promoting the bone health of postmenopausal patients in our community.

ACKNOWLEDGEMENT

I would like to thank my supervisor Dr. Ka-hing Wong, without his guidance and helping within these 4 years, my project will not be completed successfully. Dr Wong is willing to spend his treasurable time to discuss and follow up my process, give advices on the project design and improvement. Besides, I would like to thank Professor Dr. Doris Au and her team members for providing us a novel medaka fish model in studying osteogenic effect in my project.

Moreover, I would also like to thank our research team members, Dr. Chi-fai Wong, Mr. Jacky Cheung and Mr. Cheuk-hin Chan. Apart from our own team, I would also like to appreciate Dr. Kevin Kwok's group for providing materials and techniques in culturing medaka.

Last but not least, I would like to thank my parents for their encouragement when I faced difficulties and understanding of my pressure during the project. Without their caring, I cannot finish the project without any distraction.

CONTENTS

LIST OF FIGURES

LIST OF TABLES

LIST OF ABBREVIATION

ALP	Alkaline phosphatase
AR	Androgen receptor
ASTM	American Society for Testing and Materials
BCA	Bicinchoninic acid
BMD	Bone mineral density
BMP	Bone morphogenetic protein
BMSC	Bone marrow stromal cell
BSA	Bovine serum albumin
BSI	British standards institution
DDI	Double deionized water
DEPC	Diethylpyrocarbonate
DLS	Dynamic light scattering
DNA	Deoxyribonucleic acid
EDTA	Ethylenediaminetetraacetic acid
EDX	Energy-dispersive X-ray spectroscopy
ER	Estrogen receptor
ERK	Extracellular receptor kinase
FBS	Fetal bovine serum

GAPDH	Glyceraldehyde 3-phosphate dehydrogenase
GSK	Glycogen synthase kinase
HRP	Horseadish peroxidase
HRT	Hormonal replacement therapy
HR-TEM	High resolution transmission electron microscopy
ICP-MS	Inductively coupled plasma mass spectrometry
ICP-OES	Inductively coupled plasma optical emission spectrometry
ICSBP	Interferon consensus sequence binding protein
IgG	Immunoglobulin G
Ihh	Indian hedgehog homolog
IOF	International osteoporosis foundation
IR	Infrared spectroscopy
ISO	International organization for standardization
ITF-2	Immunoglobulin transcription factor 2
LDL	Low density lipoprotein
Lef	Lymphoid enhancer-binding factor
LRP	Low-density lipoprotein receptor-related protein
MAPK	Mitogen-activated protein kinase
Mdm2	Mouse double minute 2 homolog

MicroCT	Micro computed tomography
MTS	3-(4,5-dimethylthiazol-2-yl)-5-(3-carboxymethoxyphenyl)-2-(4-sulfophenyl)-2H-tetrazolium
MWCO	Molecular weight cut off
NTA	Nanoparticles tracking analysis
OCN	Osteocalcin
OPG	osteoprotegerin
Osx	Osterix
PAGE	Polyacrylamide gel electrophoresis
PCR	Polymerase chain reaction
PKC	Protein kinase C
PKD	Protein kinase D
PMS	Phenazine methosulfate
PMSF	phenylmethylsulfonyl fluoride
PSP	Polysaccharide saccharide protein complex
PTH	Parathyroid hormone
PTR	*Pleurotus tuber-regium*
qPCR	Real time polymerase chain reaction
RANKL	Receptor activator of nuclear factor kappa-β ligand

Rho	Ras homolog
RIPA	Radioimmunoprecipitation assay buffer
RNA	Ribonucleic acid
RT-PCR	Reverse transcription polymerase chain reaction
Runx2	Runt-related transcription factor 2
SAED	Selected area electron diffraction
SD rats	Sprague Dawley rats
SDS	Sodium dodecyl sulfate
Se0	Elemental selenium
SEM	Standard error mean
SeNPs	Selenium nanoparticles
SERM	Selective estrogen receptor modulator
TBST	Tris-buffer saline with tween 20
Tcf	T-cell factor
TEM	Transmission electron microscopy
TGF	Transforming growth factor
XRD	X-ray diffraction

1. Introduction and Background

1.1. Osteoporosis

Osteoporosis is medically defined as a skeleton decrease with low bone mineral density or deterioration in bone micro-architecture (**Figure 1**), leading to high risk of bone fractures in different parts of human body. Since its only observable symptom is bone fracture, osteoporosis is commonly regarded as a kind of "silent disease". In addition to elderly, postmenopausal woman is the major high-risk group of osteoporosis due to their loss of estrogen production. As reported by International Osteoporosis Foundation [1] , osteoporosis influenced 200 million women worldwide, and bone fracture commonly occurred at body parts like hip, forearm and vertebrate. Subject to the increase of world aging population, osteoporosis has become one of the major public health issues nowadays, causing significant medical & socio-economical burdens. According to IOF, the incident rate of hip fracture in men and women is projected to be increased by 310% and 240%, respectively. Thus, there is a pressing need to develop effective approaches for managing and/or preventing osteoporosis.

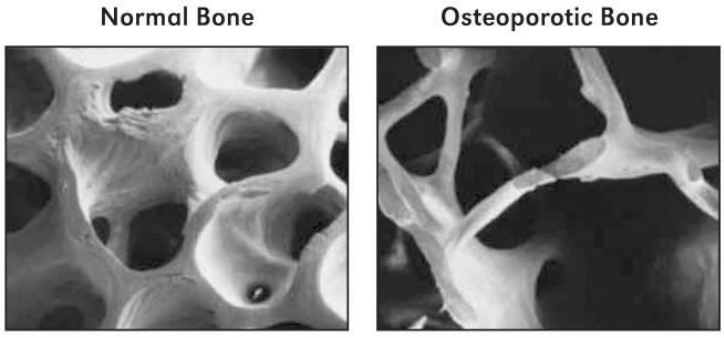

Figure 1. Micro-architecture between normal and osteoporotic bone [2]

1.2. Local Situation of Bone Health and Osteoporosis

According to the statistics released from the IOF in 2013, the life expectancy of Hong Kong population will increase from 82 to 84 years old by 2050 (**Figure 2**). Although the total population of Hong Kong will be decreased, people aged over 50 and 70 years are projected to be increased for 28% and 165% by 2050, respectively (**Figure 3)**.

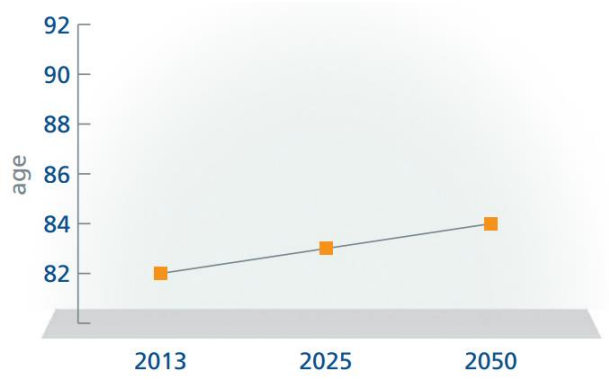

Figure 2. Life expectancy of Hong Kong population [1]

Figure 3. Projection of Hong Kong population [1]

Recently, Lau and her co-investigators [3] also indicated that despite the trend of hip fracture is decreasing, the incidence of hip fracture of last 50 years was dramatically increased by 300% from 1960's to 1990's [4].

In response to the need of health-conscious population in Hong Kong, numerous bone health products such as calcium and vitamin D supplement have been launched to local market in the past two decades. Nevertheless, a community-based study showed that the lifestyle of Hong Kong women such as insufficient physical activity and limited exposure to sunlight, significantly increased their risk to osteoporosis, resulting in a higher % of postmenopausal osteoporosis cases than that of the Western countries [5]. As reported by the Hospital Authority of Hong Kong, approximately 4,500 cases of hip fracture were received annually, causing hospital expenditure of about 52 billion USD every year. More importantly, the cost is expected to be significantly increased in the next 10 years due to the expansion of aging population in Hong Kong.

1.3. Current Medications for Osteoporosis

In order to treat osteoporosis, different medications have been released and studied. The most commonly used medications are summarized as follow:

Table 1. Summary of current medications commonly used in osteoporosis.

Name of treatment	Examples	Mechanism(s) of action	Side effect(s)	Eligible for reimbursement in Hong Kong
Bisphosphonates	Alendronate Risedronate	Inhibit bone resorption with increased BMD and reduction of bone fractures [6, 7]	Increase cardiovascular risks [8-11]	100% with prior fracture
Calcitonin	Salmon calcitonin	Inhibit osteoclast with mild increase in BMD [12]	Very rare allergic reaction; Low efficacy [12]	Only employed for pain treatment in acute vertebral fracture
Denosumab	Denosumab	Inhibit bone resorption by preventing RANKL bind to osteoclast [13]	Serious allergic reaction; Hypocalcemia [14, 15]	100% with prior fracture and intolerance to oral alendronate
Selective Estrogen Receptor Modulators (SERM)	Raloxifene Bazedoxifene	Act as estrogen agonist on bone only; Do not stimulate breast cancer in postmenopausal women [16, 17]	Myocardial infaraction; Increase risk of fatal stroke [18]	No

Strontium Ranelate	Strontium Ranelate	Slightly inhibit bone resorption and promote bone formation [19, 20]	Nausea and diarrhea; Heart attack [21]	100% with prior fracture and intolerance to oral alendronate
Teriparatide	Teriparatide	Stimulate bone formation and inhibit bone resorption [22, 23]	Osteosarcoma [24]	No
Hormone Replacement Therapy (HRT)	Estrogen Progestin	Slow down bone turnover and increase BMD in postmenopausal women [25-27]	Increase risk of cardiovascular diseases; Breast cancer [26, 28]	Yes

Table 1 showed a list of medication currently used for treating osteoporosis. In particular, hormone replacement therapy (HRT) has been widely used to alleviate the physical symptoms and to prevent clinical consequences of postmenopausal osteoporosis [29]. However, recent studies by Women's Health Initiative as well as the Million Women reported that HRT would significantly increase the risk of postmenopausal women in developing breast cancer, stroke, thrombosis and cardiovascular disease [28, 30]. Hence, there is a pressing need to develop alternative approach for managing and/or preventing postmenopausal osteoporosis.

1.4. Bone Remodeling

Bone remodeling is a lifelong process of regulating "new bone formation" and "old bone resorption" (**Figure 4**). These two sub-processes are governed by specialized cell types named "osteoblast" as well as "osteoclast" and an imbalance of which results in metabolic bone diseases like osteoporosis [31]. Substantial evidences have demonstrated that promoting bone formation is one of effective strategies to reduce the risk of first and recurrent fractures. Hence, there is a clear clinical need to develop new bone forming agents for the prevention and treatment of postmenopausal osteoporosis.

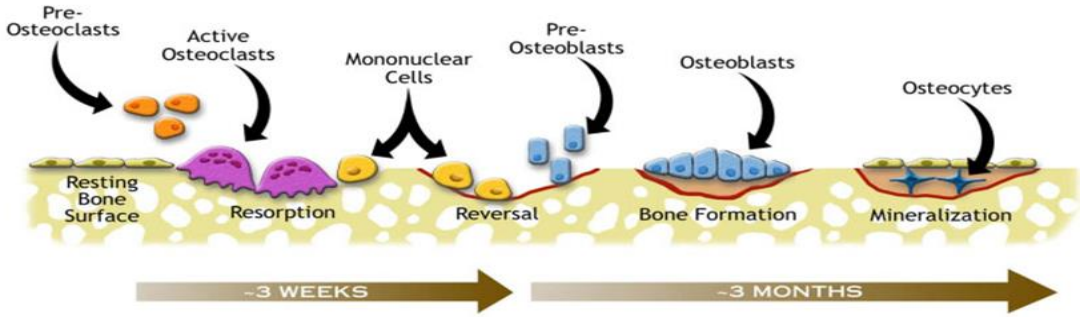

Figure 4. Bone remodeling system [32]

1.5. Osteoblastic Differentiation

Osteoblasts are derived from mesenchymal stem cells, which are also progenitors of myocytes, chondrocytes and adipocytes [33]. During osteoblastogenesis, osteoblast differentiation is one of the crucial steps (**Figure 5**). Substantial evidences have demonstrated that BMP-2 (bone morphogenetic protein-2) signaling via Smad-dependent and/or Smad-independent pathway(s) is one the most important signaling transduction cascades for regulating osteoblast differentiation [34].

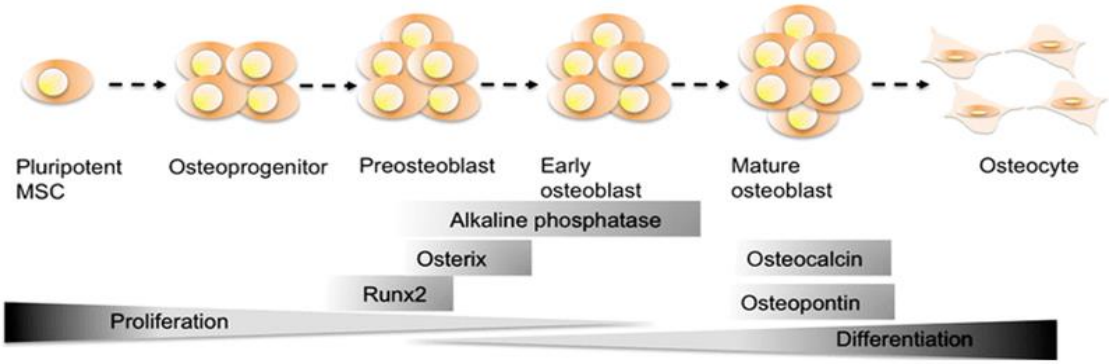

Figure 5. Osteoblastogenesis [Adopted from [35]]

1.5.1. BMP-2 signaling

BMPs are a group of phylogenetically conserved signaling molecules showed potent osteogenic effects and were initially identified by their capacity to induce endochondral bone formation [36-38]. BMP-2, -4 and -6 are the most readily detectable BMPs in osteoblast cultures [36, 39]. Different BMPs have their own unique functions in osteoblast differentiation. BMP-2, BMP-6, BMP-7 and BMP-9 have been found to promote bone formation, while BMP-3 acts as an inhibitor [40].

As shown in **Figure 6**, on receptor activation, BMP-2 transmit signals through Smad-dependent and/or Smad-independent pathways [41]. In Smad-dependent pathways, three classes of Smads are involved: (i) Receptor-regulated Smads (R-Smads), which are activated by Smad 1, 5 and 8; (ii) Common partner BMP mediator Smads (Co-Smads) such as Smad 4; and (iii) Inhibitory Smads (I-Smads) such as Smad 6 and 7. Upon ligand stimulation and activation by type II receptors, type I receptors phosphorylate R-Smad followed by forming complexes with Co-Smads [42]. The R-Smad/Co-Smads complexes will then translocate into the nucleus, regulating the transcription of target genes by interacting with various transcription factors and transcriptional coactivators or co-repressors. I-Smads will

negatively regulate signaling by the R-Smads and Co-Smads. Upon BMP-2 signaling activation, R-Smads and Runx2 physically interact with each other and co-operatively regulate the transcription of target genes, leading to osteoblast differentiation of mesenchymal progenitor cells [43-45]. Interestingly, through the action of R-Smads, BMP does not induce the Runx2 expression in the mesenchymal progenitor cells directly. Instead, it facilitates the expression of Dlx5 [46, 47], which will then indirectly promote the Runx2 expression in osteoprogenitor cells. Previous studies also discovered that transcription factors including Hey1 (also termed HesR1 and Herp2), Tcf7, ITF-2, and ICSBP were specifically expressed in osteoblast cells by BMP-2 treatment, involving both Notch and Wnt signaling [48, 49].

In Smad-independent pathway, BMP-2 has been reported to activate MAP kinases such as ERK, JNK and p38 in osteoblastic cells, regulating alkaline phosphatase (ALP) and osteocalcin (OCN) expressions [50, 51]. It is worth noting that BMP-2 was found to activate JNK and p38 via protein kinase D (PKD) during osteoblastic differentiation, independent of protein kinase C (PKC) activity [52]. Previous studies also reported that Smad and p38 MAPK pathways converged at the Runx2 to regulate cell differentiation [53] and Runx2 plays a central role in the BMP-2-induced differentiation of C2C12 cells, diverting them from myogenic to

osteogenic pathway [54, 55]. Similar to Smad-dependent pathway, the homeobox gene Dlx5 is an upstream target of Smad-independent pathway, stimulating the downstream transcription factor, Runx2 followed by upregulating bone-specific genes during osteoblastic differentiation [47]. In addition to Runx2, BMP-2 has been found to promote osterix (Osx) expression in mouse progenitor cells and chondrocytes mediated by Dlx5 but is independent of Runx2 [56-58]. Interestingly, this BMP-2 inducing effect was mediated via p38 but not via ERK. Nevertheless, under osteogenic culture conditions, both ERK and p38 were involved in mediating the Osx expression [59].

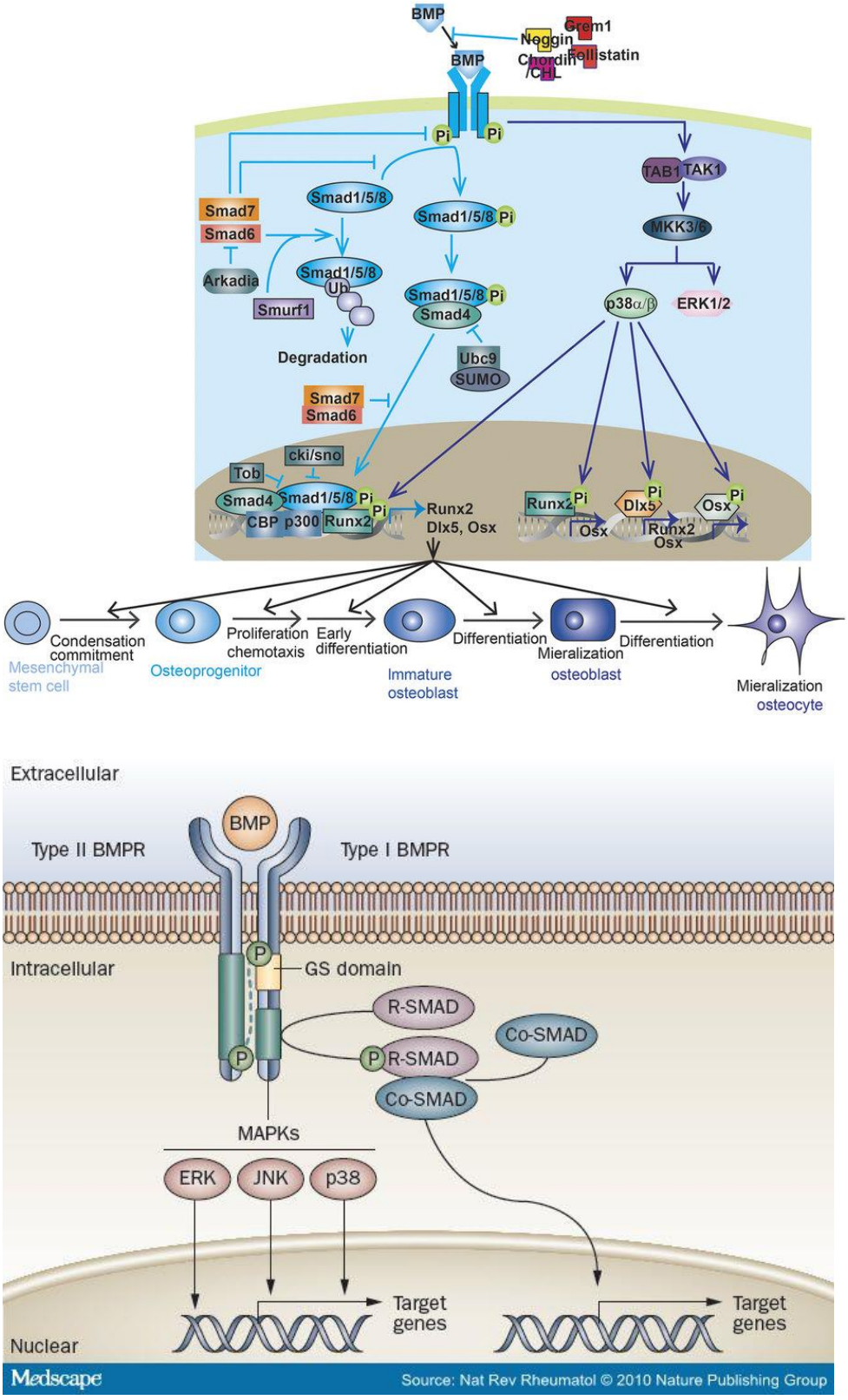

Figure 6. BMP-2 signaling pathway [60, 61]

1.6. Experimental Design

Selenium (Se) is an essential trace mineral to human health with a recommended daily allowance of 55μg/day for adults [62]. Physiologically, Se is an important constituent of selenoproteins (e.g. thioredoxin reductase), which are important anti-oxidant enzymes to help protect the body from cellular damage by free radicals, supporting our immune system, cell proliferation and differentiation.[63-66]. In the past decades, substantial evidences have demonstrated that Se deficiency is detrimental to bone micro-architecture and associated with osteopenia, osteoporosis as well as Kashin-Beck osteoarthropathy [64, 67, 68], suggesting its crucial role in bone metabolism. Previous studies also indicated that Se supplementation could not only restore the anti-oxidative capacity and prevent cell damage in bone marrow stromal cells, but also protect their osteoblastic differentiation inhibited by H_2O_2 via suppressing oxidative stress and ERK signaling pathway [69].

The efficacy and toxicity of Se are highly dependent on its chemical form and dosage. Recently, Se nanoparticles (SeNPs) have become the new research target, since they were found to possess remarkable anti-cancer efficacy and low toxicity [70, 71] compared to those organic and inorganic selenocompounds. Apart from toxicity evaluation [72, 73] as well as chemical and bio-synthesis [74, 75], the *in vitro* anti-tumor

efficacy of SeNPs have been widely reported in literature for the past ten years [76-78]. Although SeNPs stabilized with glutathione and bovine serum albumin have been recently found to promote the growth of primary human calvarial osteoblasts and alleviate the bone loss in ovariectomized rats, scientific research concerning the effects of SeNPs on bone health is still very limited. Besides, SeNPs aggregate easily and their health-promoting effects will be significantly reduced, once their nano size could not be maintained. This limiting factor has attracted many scientists to search for novel biomolecules that could stabilize the SeNPs without compromising their health-promoting effects.

Pleurotus tuber-regium (Fr.) Singer (also known as "tiger milk mushroom" in China), is an edible and medicinal mushroom mainly distributed in tropical and subtropical regions such as China, Australia and Nigeria [79]. This basidiomycete is the only *Pleurotus* species that can produce mushroom sclerotium [80]. Although this white-rot fungus is widely used for food and medicinal purposes in Nigeria, it is under-utilized in Asia and its large-scale cultivation is not currently available [81]. By using its water-soluble polysaccharide-protein complex (PSP), we have successfully prepared novel SeNPs (PTR-SeNPs) under a simple redox system. In contrast to normal cells, PTR-SeNPs were found to significantly inhibit the growth of human

breast carcinoma MCF-7 cells (IC_{50}=3.7μM) by apoptosis induction via activating a ROS-mediated mitochondrial pathway [82]. Comparing with the IC_{50} value of native SeNPs (200μM) and mushroom PSP (400 μg/mL), interestingly, the mushroom PSP surface decoration did not only stabilize the SeNPs, but also significantly enhance their cellular uptake and anti-proliferative effect on the MCF-7 cells [82].

Thus, in order to figure out whether PTR-SeNPs could be developed into a novel bone forming agent for prevention and treatment of osteoporosis, in this project, the *in vitro* and *in vivo* effects of PTR-SeNPs on bone formation were further investigated using the following approaches and a project summary is shown in **Figure 7**:

1.6.1. To investigate the direct effects of PTR-SeNPs on bone formation in vitro

Preosteoblast murine MC3T3-E1 subclone 4 cells (ATCC; CRL-2593) is one of *in vitro* models widely used for studying bone formation [83]. In this study, a dose- and time-dependent study of the osteogenic effect of PTR-SeNPs (including cell proliferation, osteoblast differentiation and bone mineral formation) on MC3T3-E1 cells was performed. The effective dosage of PTR-SeNPs for the MC3T3-E1 cells was firstly determined and then applied in the time-dependent studies.

1.6.2. To elucidate the mechanism of action of PTR-SeNPs on bone formation in vitro

Substantial evidences have demonstrated that BMP-2 signaling via Smad-dependent and/or Smad-independent pathway(s) is one the most important signaling cascades in regulating osteoblastogenesis (bone formation) [34]. Upon cell surface ligand binding, BMP-2 forms a hetero-tetrameric receptor complex with the dimers of both type II and type I transmembrane serine/threonine kinases, triggering phosphorylation of Smad1/5/8 in the cytoplasm. Phosphorylated Smad1/5/8 then forms a trimetric complex with Smad4 followed by translocation to nucleus, where they regulate the transcription of target genes for osteoblast differentiation. In particular, homeobox gene Dlx5, which is an upstream target of both BMP-2/Smad

dependent and BMP-2/Smad independent pathways, plays a pivotal role in stimulating the downstream transcription factors such as Runx2 and Osx [34]. MAPKs (including ERK, p38 and JNK) signaling, which are upstream regulators of Dlx5 in the BMP-2/Smad independent pathway, has been found to play important role in osteoblast differentiation, regulating the ALP, Runx2 and OCN expressions [34]. Interestingly, the involvement of BMP-2/Smad dependent pathway in SeNPs mediated osteoblast differentiation has been recently reported [84]. Thus, in this study, we investigated whether PTR-SeNPs mediated osteoblastogenesis is related to BMP-2 signaling like other SeNPs using the MC3T3-E1 cells. In addition to BMP-2, a time-dependent study on the gene expression of major osteogenic markers (such as Dlx5, ALP, Runx2, Osx, OCN and OPG/RANKL) as well as protein expression and phosphorylation of Smad1/5/8 triggered by the PTR-SeNPs was performed in the MC3T3-E1 cells by qPCR and Western blotting, respectively. Besides, in order to determine the role of MAPKs signaling in the PTR-SeNPs mediated osteoblast differentiation, a time-dependent study on the protein expression and phosphorylation of ERK, p38 and JNK triggered by the PTR-SeNPs was also conducted in the MC3T3-E1 cells.

1.6.3. To study the cellular uptake behavior of PTR-SeNPs

Endocytosis has been widely reported as the major cellular uptake mechanism for nanoparticles [85]. Interestingly, our preliminary study found that after cellular internalization, coumarin-6 labelled PTR-SeNPs (120μM) co-localized with lysosomes in the MCF-7 human breast carcinoma cells round 10 min [82]. Similarly, in this study, the cellular uptake behavior of PTR-SeNPs by the MC3T3-E1 cells was traced intracellularly by fluorescence microscopy.

1.6.4. To evaluate the effects of PTR-SeNPs on bone formation in vivo

Rat and mouse are commonly used animal models for bone formation study [86-89]. Due to space requirement and time consuming, teleost fish such as zebrafish and medaka have been suggested previously to study bone metabolism in limited space [90]. Similar to mammals, the bone matrix of teleost fish is synthesized by osteoblasts in the presence of osteocyte [91, 92] and undergoes resorption by multinucleated osteoclasts [93]. More importantly, mammalian's bone remodeling markers and transcription factors such as alkaline phosphatase, tartrate-resistant phosphatase, runx2, twist, col10a1 and osterix were all found in teleost fish with similar structure and function[90, 92, 94-96]. Compared to the rat and mouse models, advantages of using fish model include short experimental period, less space requirement and sample use as well as large sample size and cost effective.

Research studies on aging and bone metabolism using Japanese medaka (*Oryzias latipes*) as animal model have been reported previously [4]. In this project, we established a brand new *in vivo* screening model to investigate the effect of PTR-SeNPs on bone formation using medaka larvae. In brief, a time dependent study on the vertebrae development (both bone and cartilage) of medaka larvae after feeding PTR-SeNPs for 11 days was visualized by Alizarin Red S and Alcian Blue double staining. Besides, the gene expression of major osteogenic markers such as ALP, Runx2, Osx and OPG/RANKL induced by PTR-SeNPs was also being determined.

We anticipate that findings of this study could provide significant insights into the *in vitro* and *in vivo* effects of PTR-SeNPs on bone formation. Our long-term goal is to develop an evidence-based bone-forming agent for promoting the bone health of postmenopausal patients in our community.

1.7. Hypothesis

a) PTR-SeNPs could induce bone formation on preosteoblast MC3T3-E1 cells via BMP-2 signaling cascades

b) PTR-SeNPs would enter the MC3T3-E1 cells via endocytosis

c) PTR-SeNPs could stimulate bone formation in Japanese medaka larvae

1.8. Objectives

a) To characterize the direct effects of PTR-SeNPs on bone formation using preosteoblast MC3T3-E1 cells

b) To investigate the BMP signaling cascades modulated by PTR-SeNPs during osteoblast differentiation using MC3T3-E1 cells

c) To study the cellular uptake behavior of PTR-SeNPs by the MC3T3-E1 cells

d) To investigate the stimulatory effect of PTR-SeNPs on bone formation using Japanese medaka larvae

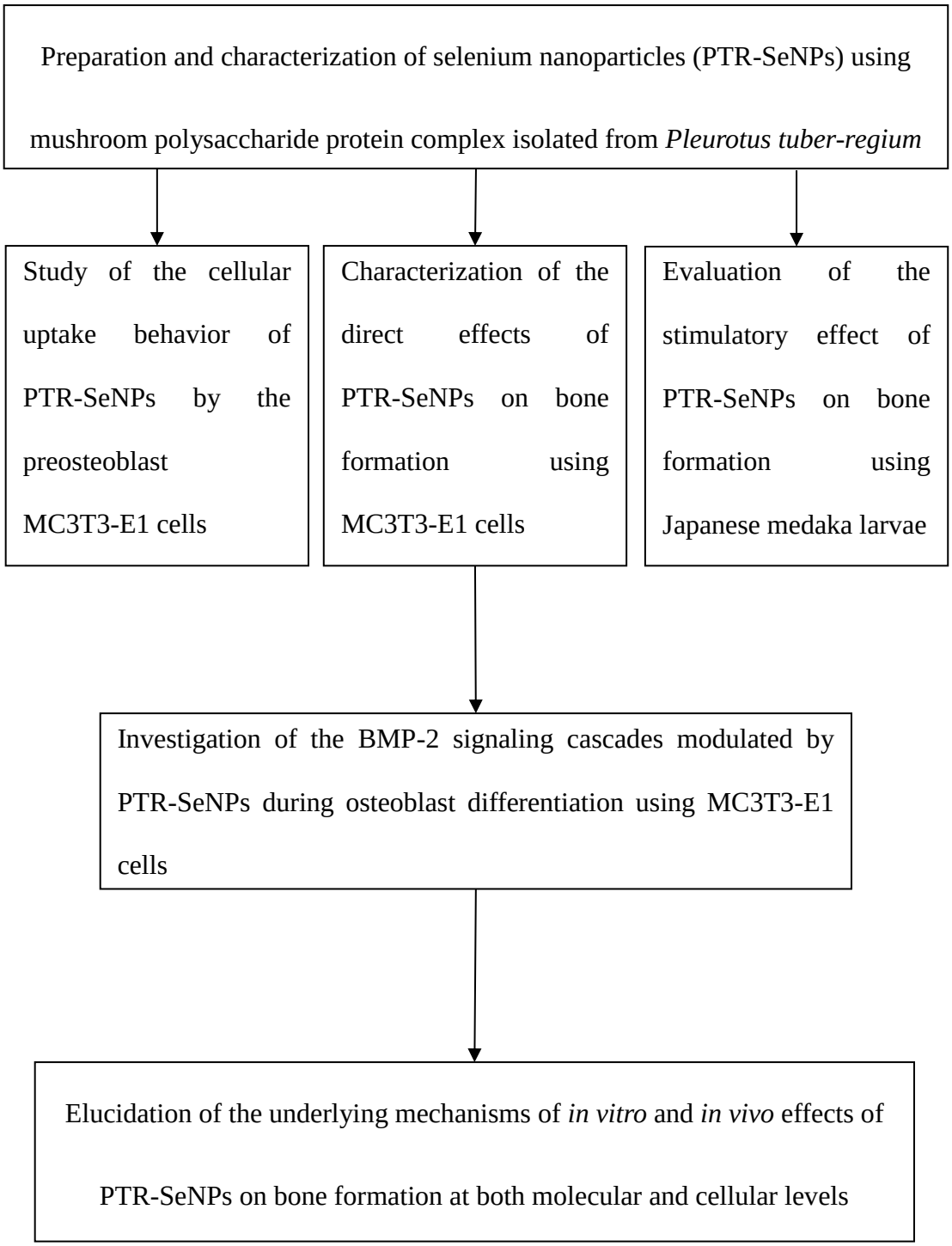

Figure 7. Project Summary

2. Materials and Methods

2.1. Chemicals and Reagents

All chemicals were at least analytical grade and purchased from Sigma-Aldrich Co. (St. Louis, MA, USA) unless specifically stated.

2.2. Mushroom Samples

Mushroom sclerotia of *P. tuber regium* were obtained from Sanming Mycological Institute in the Fujian Province of China. All sclerotia were cleaned with minimum amount of ultra-pure water to remove the dust and soils adhered on their surfaces before air-drying. The rinds (outer covering) of sclerotia were then removed in order to avoid any contamination that might come from the compost as well as the wrapping plastics bag during cultivation. All sclerotia were pulverized to pass through a screen with an aperture of 0.5 mm using a cyclotech mill (Tecator, Höganäs, Sweden). The milled mushroom powders were then transferred to airtight plastic bags and stored in a desiccator at room temperature (24 °C) prior to further polysaccharide protein complex extraction.

2.3. Hot Water Extraction of Mushroom Polysaccharide Protein Complex

About 500g of sclerotial powders were used for hot water extraction at 95-100°C for 2 hours with a sample-to-solvent ratio of 1:20 (w/v). After cooling, the extract was centrifuged at 18,600 x g for 1 hour at 4^{o}C and the supernatant was collected. The whole extraction process was repeated twice and all supernatants were pooled together followed by rotary evaporation (60^{o}C) and centrifugation under the same conditions. Subsequently, the concentrated supernatant was dialyzed using Spectra/Por® Dialysis Membrane (*M*w cutoff: 8,000) until the total dissolved solute (TDS) was similar to that of Milli-Q water. Dialyzate, which is the hot water soluble polysaccharide protein complex (PSP) was then freeze dried into powder by FreeZone 6L Console Freeze Dry Systems with Stoppering Tray Dryers (Labconco, USA) and stored in desiccator prior to selenium nanoparticles preparation.

2.4. Preparation of PTR-SeNPs

According to our award-winning and patented nanotechnology, 10mL of PTR-SeNPs were prepared by standardized procedures using the hot water-soluble PSP. In brief, 4mL of aqueous PSP (1.5mg/mL) was mixed with 1mL of aqueous sodium selenite (25mM) under magnetic stirring for 2 hours before drop-wise addition of 1mL of freshly prepared ascorbic acid (100mM). After reconstituting with ultrapure water to

10mL, the mixture was stirred for 10 min under room temperature and allowed to react for 24 hours at 4^{o}C before extensive dialysis (*M*w cutoff: 8,000) until the TDS was similar to that of Milli-Q water. The resulting dialysate, which is the PTR-SeNPs was stored at 4^{o}C prior to further composition analysis and structure characterization.

2.5. Composition Analysis and Structure Characterization of PTR-SeNPs

2.5.1. Selenium concentration of PTR-SeNPs

In brief, 0.5mL of PTR-SeNPs was mixed with 10mL of trace metal grade 70% concentrated nitric acid followed by microwave digestion with ETHOS One Advanced Microwave Digestion System (Milestone S.r.l., Italy), using a temperature program of initial temperature 180^{o}C with a hold of 20 min followed by a temperature rise to 250^{o}C with a final hold of 30 min. Digestate was then transferred into a volumetric flask and marked up to 25mL using Milli-Q water. After filtered with 0.45µm cellulose acetate syringe filter, the Se concentration of filtrate was determined by Agilent 710 ICP-OES (Agilent Technologies Inc., USA) using 196.026 as emission wavelength and 203.985 as reference. For quantification, a standard curve of selenium ranging from 0.1ppm to 5ppm was prepared.

2.5.2. Particles size and stability of PTR-SeNPs

In brief, PTR-SeNPs was diluted 1,000 folds followed by injection into Nanosight NS300 (Malvern Instruments Ltd., UK) for particles size determination using nanoparticles tracking analysis (NTA). To investigate its stability, PTR-SeNPs, nanoparticles was stored at 4^{o}C and samples were collected for every 2 weeks prior to particles size determination using the Nanosight NS300.

2.5.3. Structure characterization of PTR-SeNPs using HR-TEM-EDX

In short, 30µL of PTR-SeNPs was firstly dropped onto a hollow carbon grid and air-dried. The whole procedure was repeated for 5 times. The particle size of specimen was then visualized by JEM-2100F Field Emission Electron Microscope (JEOL Ltd., Japan) with magnification of 20,000×, 40,000× and 150,000× using 200kV electrons beam. Subsequently, single nanoparticle was selected under magnification of 150,000× and its elemental composition and crystal structure were further investigated by using HR-TEM-EDX (JEOL JEM-2100F + Horiba EX-250). All images obtained were analyzed by software ImageJ.

2.5.4. Structure interaction between SeNPs and PTR-PSP

In brief, PTR-PSP and freeze-dried PTR-SeNPs were individually ground into powder together with potassium bromide under humidity-controlled environment. Subsequently, pellet discs of each powder mixture were prepared and their Infrared spectra were determined and compared by using Nicolet™ iS™ 50 Fourier Transform Infrared Spectrometer (FT-IR) in order to figure out the major functional groups that are responsible for the association between PTR-PSP and SeNPs.

2.6. Cell Culture

MC3T3-E1 subclone 4 preosteoblast cells were purchased from American Type Culture Collection (ATCC ® CRL-2593, Rockville, MD, USA) and maintained in ascorbic acid free α-Minimum Essential Medium (α-MEM; Invitrogen, San Diego, CA, USA) supplemented with 10% fetal bovine serum (FBS; Invitrogen, San Diego, CA, USA), 1% 100× antibiotics and anti-mycotics (Invitrogen, San Diego, CA, USA) in a 37^{o}C incubator with 95% relative humidity and 5% CO_2. Cells were routinely passaged using 0.25% trypsin/0.1% EDTA at 70 – 90% confluence.

2.7. Direct Effects of PTR-SeNPs on Bone Formation

2.7.1. Cell proliferation assay

In brief, MC3T3-E1 cells were firstly seeded into 96-well tissue culture plates at 15,000 cells/well. Cells pretreated with different concentrations of PTR-SeNPs (10nM - 10µM), 6µg/mL PTR-PSP or 10µM sodium selenite were then incubated for 24, 48 and 72 hour followed by determining cell proliferation using MTS [3-(4,5-dimethylthiazol-2-yl)-5-(3-carboxymethoxyphenyl)-2-(4-sulfophenyl)-2H-tetr azolium] assay (Promega). To perform MTS assay, 4.6 mg of phenazine methosulfate (PMS) was dissolved in 5mL of PBS, while 42mg of MTS powder was dissolved in 21mL of PBS with pH adjustment to 6.0 – 6.5. Subsequently, 4.2 mL of MTS solution was mixed with 1mL of PMS solution. After filtered with 0.22µM filter, cells were added into the MTS/PMS mixture (20µL/well) and incubated for 1 – 2 hours at 37^{o}C in a humidified incubator with 5% CO_2. Absorbance was determined at 490nm using a microplate reader (Clariostar, USA).

2.7.2. Osteoblastic differentiation

To study osteoblastic differentiation, MC3T3-E1 preosteoblast cells cultured in osteogenic medium containing 10nM β-glycerophoshpate and 50 μg/mL ascorbic acid were pretreated with 10μM of PTR-SeNPs for 7 days. ALP activity in the MC3T3-E1 cells was then determined by spectrophotometry at 410 nm, while ALP-containing cells (osteoblasts) were visualized by ALP staining kit. Fresh culture media were replenished every 3 – 4 days.

2.7.2.1. ALP activity

In brief, MC3T3-E1 cells pretreated with 10μM of PTR-SeNPs for 7 days were washed with PBS followed by lysed with 50mM Tris-HCl (200μL/well, pH 8.0) and 0.5% Triton X-100. Cell lysates were then harvested and transferred into 1.5mL centrifuge tubes before storage at -80^{o}C. After defrosted, all lysates were centrifuged (21,000 × g; 20 min; 4^{o}C) and 10μL of supernatant was added into 96 wells in triplicate followed by incubation with 200μL of 10mM *p*-nitrophenyl phosphate (*p*NPP) in 1M diethanolamine and 0.5mM $MgCl_2$ (pH 9.8) for 15 – 30 min. Consequently, the reaction was quenched by adding 50μL of 3M NaOH and the resulting absorbance was measured at 410nm using a microplate reader. To normalize the ALP activity, the total protein content was also determined by BCA assay. In short, 200μL of BCA solution (mixing BCA reagent A with B as indicated in manufacture's manual) was

added into a well containing 2µL of protein sample and 23µL of water followed by incubation at 37^{o}C for 30 min. Similarly, the resulting absorbance was measured at 595nm using a microplate reader.

2.7.2.1. ALP staining

In brief, MC3T3-E1 cells pretreated with 10µM of PTR-SeNPs for 7 days were washed with PBS and fixed with 10% formalin for 15 min. The ALP in cells were then stained by Fast Blue RR salt and Naphthol AS-MX phosphate alkaline solution for 60 min followed by rinsing thoroughly with deionized water.

2.7.3. Mineralization assay

To study bone mineral formation, MC3T3-E1 cells cultured in osteogenic medium containing 10nM β-glycerophoshpate and 50µg/mL ascorbic acid were pretreated with different concentration of PTR-SeNPs (10µM) for 16 days. Bone nodules formed in the MC3T3-E1 cells were then visualized and compared by Von Kossa and Alizarin Red S staining.

2.7.3.1. Von Kossa staining

To detect calcium deposit, cells were pre-washed with PBS and fixed with 10% formalin for 15 min. Fixed cells were then treated with 5% silver nitrate for 30 min

under light following by sequential washing with deionized water, 5% sodium carbonate in 10% formalin (1 min), deionized water and 5% sodium thiosulfate (5 min). Consequently, stained well was captured and analyzed by ImageJ to quantify calcium deposition.

2.7.3.2. Alizarin Red S staining

Similarly, cells were pre-washed with PBS and fixed with 10% formalin for 15 min. Fixed cells were then stained with 40nM Alizarin Red S solution (pH 4.1) for 20 min with gently shaking followed by heavy washing 4 times with 4mL of deionized water for 5 min per well. Excessive water in the wells was removed and the resulting image was captured. To quantify the calcium deposit, 800µL of 10% (v/v) acetic acid was added into each well followed by incubation with shaking for further 30 min. All stained cells were then scraped with cell scraper and transferred into a 1.5mL centrifuge tube using acetic acid. After vortex-mixing for 30 sec, 500µL of mineral oil was added and the slurry was heated up to 85^{o}C for 10 min followed by cooling down in ice for 5 min. All tubes were then centrifuged at 20,000 × g for 15 min and 500µL of the supernatant was transferred into new Eppendorf tubes. After adding 200µL of 10% (v/v) ammonium hydroxide, the mixture was aliquot in a 96 well plate in triplicate followed by measuring the absorbance with a microplate reader at 405nm.

2.7.4. Total RNA isolation

To further characterize the direct effects of PTR-SeNPs on osteoblastogenesis, mRNA expression of major osteogenic markers (such as ALP, Dlx5, Runx2, Osx, OCN and OPG/RANKL) in the MC3T3-E1 cells pretreated with 10µM of PTR-SeNPs for 3, 7 and 16 days were quantified by real-time PCR. For total RNA extraction, cells were washed twice with 1mL of ice cold PBS and total RNA was isolated with 1mL of Trizol reagent per 6 wells according to manufacturer's protocol (Life technologies, USA). After homogenization, 200µL of chloroform was added with gentle shaking and the mixture was allowed to stand for 3 min at room temperature. All samples were then centrifuged (12,000 × g; 10 min; 4^{o}C) and the top aqueous layers were transferred into new tubes prior to adding 500µL of 2-propanol. Subsequently, the whole reaction mixture was centrifuged under the same conditions and the 2-propanol was removed followed by washing with 1mL of 75% ethanol in DEPC H_2O. After centrifugation (7,500 × g; 5 min; 4^{o}C), the 75% ethanol was removed and the RNA pellet was air-dried. Once the RNA pellets turned into milky, 10 - 20µL of DEPC H_2O was added to re-dissolve the RNA and stored at -80^{o}C until further qPCR analysis.

2.7.5. Real-time polymerase chain reaction (qPCR)

In brief, 20ng of RNA was firstly prepared by One-Step SYBR Green RT-qPCR according to manufacturer's instructions. In a 20µL reaction, the reaction mixture

contained 10µL of 2X One Step SYBR RT-PCR Buffer 4, 0.8µL of PrimeScript One-Step Enzyme Mix 2, 0.4µM of Forward PCR primers, 0.4µM of Reverse PCR primers and 20ng of RNA sample. qPCR analysis of BMP-2 and major osteogenic markers (such as ALP, DLx5, Runx2, Osx, OCN and OPG/RANKL) was performed by a Pikoreal thermal cycler system (Thermo, USA) using thermal cycling program and primers shown in **Table 2** and **3**, respectively. Relative mRNA expression of each osteogenic marker gene was normalized to that of GAPDH.

Table 2. Thermal cycling program of qPCR analysis (mouse)

Stage	**Temperature**	**Hold Time**
Reverse transcription (1 cycle)	42 ^{o}C	5 min
	95 ^{o}C	10 sec
PCR reaction (40 cycle)	95 ^{o}C	5 sec
	60 ^{o}C	20 sec
Melting curve analysis	95 ^{o}C	0 sec
	65 ^{o}C	15 sec
	95^{o}C	0 sec

Table 3. Primer list for qPCR analysis (mouse)

Gene	**Forward Primer (5' – 3')**	**Backward Primer (5' – 3')**
Runx2	AAGTGCGGTGCAAACTTTTCT	TCTCGGTGGCTGGTAGTGA
ALP	AACCCAGACACAAGCATTCC	GAGAGCGAAGGGTCAGTCAG
Dlx5	GTTTCAGAAGACTCAGTACCT	TGACTGTGGCGAGTTACAC
BMP2	CCCCAAGACACAGTTCCCTA	GAGACCGCAGTCCGTCTAAG
Osx	AGAGGTTCACTCGCTCTGACGA	TTGCTCAAGTGGTCGCTTCTG
OCN	TAGTGAACAGACTCCGGCGCTA	TGTAGGCGGTCTTCAAGCCAT
OPG	ACGAACTGCAGCACATTTGG	TGTTTCCGGAACACACGTTG
RANKL	ACGCCAACATTTGCTTTCGG	ATTGCCCGACCAGTTTTTCG
GAPDH	CATGGCCTTCCGTGTTCCTA	CCTGCTTCACCACCTTCTTGAT

2.7.6. Total protein extraction

With a purpose to dissect the BMP-2 signaling (both Smad dependent and independent pathways) mediated by PTR-SeNPs during osteoblast differentiation, protein expression and phosphorylation of Smad1/5/8 ERK, p38 and JNK in the MC3T3-E1 cells pretreated with 10μM of PTR-SeNPs for 4 days were determined by Western blot analysis. For total protein extraction, cells were washed twice with PBS and lysed with 50μL of RIPA Lysis buffer containing PMSF and 1X protease and phosphatase inhibitor cocktail. Cells were then scraped and transferred into 1.5mL centrifuge tubes followed by sonication (1 min) and centrifugation (22,000 × g; 20 min; 4^{o}C). Protein content of the supernatant was determined by BCA protein assay. After mixed with 5X sample buffer, the reaction mixture was heated up to 95^{o}C for 5 min and stored at -20^{o}C prior to Western blot analysis.

2.7.7. Western blot analysis

For Western blotting, 40μg of protein sample was loaded and separated by 10% SDS-PAGE using gel electrophoresis. Separated proteins were then transferred to PVDF membranes using iBlot 2 Dry Blotting System. After blocking with 5% BSA (w/v) or 5% blocking grade non-fat dry milk powder (Bio-rad, USA) in Tris-buffered saline containing 0.1% (v/v) Tween-20 (TBST) for 1 hour at room temperature, all

membranes were incubated with specific primary antibodies including p-Smad 1/5/8, Smad 1/5/8, p-ERK, ERK, p-p38, p-38, p-JNK, JNK and GAPDH [dilution: 1:1000; 5% BSA in TBST] at 4^{o}C overnight. Subsequently, all membranes were extensively washed with TBST and incubated with the secondary anti-mouse IgG HRP-linked antibodies at 1:2000 dilution for 1 hour at room temperature. Finally, the membranes were further washed with TBST, while chemiluminescence for detection was developed using EMD Millipore Immobilon Western Chemiluminescent HRP substrate (Millipore, USA) according to the manufacturer's instructions. Image acquisition was performed using Azure^{TM} c600 digital imager (Azure Biosystem Inc., USA) followed by quantification with ImageJ.

2.7.8. Cellular uptake behavior of PTR-SeNPs

In brief, MC3T3-E1 cells were firstly seeded in a 35mm confocal dish for 24 hours followed by sequential staining with Hochest 33342 (1µg/mL; nucleus; Invitrogen, CA, USA) and Lysotracker Deep Red (75µM; lysosomes; Invitrogen, CA, USA) for 20 and 30min, respectively. After further incubation with 10µM of coumarin-6-loaded PTR-SeNPs at 37°C for 10 min, the cellular uptake behavior of PTR-SeNPs by MC3T3-E1 cells was intracellularly traced by fluorescence microscopy.

2.8. Japanese Medaka

Orange-red, outbred line of Japanese medaka (*Oryzia latipes*) was originated from the Molecular Aquatic Toxicology Laboratory of Duke University. A brood colony was maintained at 100-200 individuals (60-80 fish × 3 tanks) at any given time. This brood colony produced all the embryos for the project. In brief, adult fish in brood colony was maintained at 25^{o}C at 14:10 light/dark cycle to provide favorable conditions for egg laying. Under this condition medaka fish produce eggs daily. Fifty percent of tank water was changed daily with de-chlorinated tap water and was maintained at pH 8.0 and 30% salinity. Water pH and temperature was monitored daily; nitrate, nitrite, ammonia and water hardness were checked every month. Fish were fed twice daily with commercial fish feed, Otohime β1 (Nisshin Co, Japan), and supplemented with hatched brine shrimp *Artemia nauplii* (Lucky Brand, O.S.I., USA) for 3 days per week. Embryo less than 4 hours post-fertilization was collected and transferred to a petri dishes containing de-chlorinated water for culturing.

2.8.1. Japanese medaka embryo culture

All collected medaka embryos were firstly cultured in a petri dish using saturated sea salt water for 1 day-disinfection followed by culturing in de-chlorinated water. Embryos were cleaned and dead eggs were pick out every day

during change of water in order to prevent contamination. Embryos were cultured at 25 – 30^{o}C until hatched and larvae were transferred to new containers before performing PTR-SeNPs exposure experiment.

2.8.2. Fish diet preparation

In brief, 10 g of commercial fish feed (Otohime β1) was firstly mixed with 10mL of PTR-SeNPs to make a PTR-SeNPs based diet containing 10 ppm Se. After freeze-drying, the PTR-SeNPs based diet was grinded by using mortar and pestle to pass through a 100µm sieve. For control diet, 10mL of MilliQ water was used instead. Final Se concentration of both control and SeNP-based diets were measured by ICP-MS before use.

2.8.3. PTR-SeNPs exposure experiment using medaka larvae

After collecting the 5 days post-hatched medaka larva, both control and PTR-SeNPs treatment groups were cultured in 6-well cell-culture plates (one medaka larvae per well) and fed the control or PTR-SeNPs based diet (10ppm) twice daily for a total of 11 days. During fish sampling, medaka larvae were anaesthetized by immersing in ice-cold aquarium water for 30 sec.

Similar to the *in vitro* study, the mRNA expression of major osteogenic markers (such as ALP, Runx2, Osx and OPG/RANKL) in the medaka larvae fed with 10ppm of PTR-SeNPs for 2 days were quantified by qPCR. As mentioned in 2.7.4 and 2.7.5, total RNA isolation from medaka larvae (n=3) were performed using Trizol reagent followed by One-Step SYBR Green RT-qPCR analysis using Pikoreal thermal cycler system (Thermo, USA). Thermal cycling program and primers used are shown in **Table 2** and

Table 5, respectively. Relative mRNA expression of each osteogenic marker gene was normalized to that of 18S.

2.8.4. Bone mineralization of medaka larvae

Mineralization is the end point of bone formation. Bone and cartilage in medaka larvae after treatment with 10ppm of PTR-SeNPs for 11 days (n = 6) were double-stained by Alizarin Red S and Alcian Blue. In brief, medaka larvae were firstly fixed in 10% formalin (2 hours) followed by dehydration using 50% ethanol (10 min). After washing three times with PBS (10 min), medaka larvae were stained overnight with 0.02% Alcian blue 8GX in 70% ethanol containing 0.06M $MgCl_2$. Subsequently, medaka larvae were washed three times with absolute ethanol (10 min) followed by sequential washing with 90%, 75% 50%, 25% ethanol and finally PBS (20 min each). After bleaching with 1.5% H_2O_2 in 1% KOH (40 min) and washing three time with PBS (10 min), medaka larvae were further digested with 1% trypsin solution in 30% saturated sodium borate solution (40 min). For bone staining,

digested larvae were washed three times with PBS (10 min) and stained with saturated Alizarin Red S in 0.5% KOH overnight followed by de-staining three times with 0.5% KOH (10 min). After sequential washing with 20% glycerol/0.25% KOH and 50% glycerol/0.25% KOH, all medaka larvae specimens were stored in 100% glycerol at 4^{o}C prior to examination using stereomicroscope Nikon SMZ18 and upright microscope Eclipse Ci-E.

2.8.5. Total RNA isolation

To further characterize the direct effects of PTR-SeNPs on osteogenesis *in vivo*, mRNA expression of major osteogenic markers (such as ALP, Runx2, Osx and OPG/RANKL) in medaka larvae pretreated with 10ppm of PTR-SeNPs for 2 days were quantified by real-time PCR. For total RNA extraction, total RNA of 3 larvae were isolated with 1mL of Trizol reagent according to manufacturer's protocol (Life technologies, USA). After homogenization, 200µL of chloroform was added with gentle shaking and the mixture was allowed to stand for 3 min at room temperature. All samples were then centrifuged (12,000 × g; 10 min; 4^{o}C) and the top aqueous layers were transferred into new tubes prior to adding 500µL of 2-propanol. Subsequently, the whole reaction mixture was centrifuged under the same conditions and the 2-propanol was removed followed by washing with 1mL of 75% ethanol in

DEPC H_2O. After centrifugation (7,500 × g; 5 min; 4^oC), the 75% ethanol was removed and the RNA pellet was air-dried. Once the RNA pellets turned into milky, 10 - 20µL of DEPC H_2O was added to re-dissolve the RNA and stored at -80^oC until further qPCR analysis.

2.8.6. Real-time polymerase chain reaction (qPCR)

In brief, 50ng of RNA was firstly prepared by One-Step SYBR Green RT-qPCR according to manufacturer's instructions. In a 20µL reaction, the reaction mixture contained 10µL of 2X One Step SYBR RT-PCR Buffer 4, 0.8µL of PrimeScript One-Step Enzyme Mix 2, 0.4µM of Forward PCR primers, 0.4µM of Reverse PCR primers and 20ng of RNA sample. All qPCR analysis of those major osteogenic markers (such as ALP, Runx2, Osx and OPG/RANKL) was performed by a Pikoreal thermal cycler system (Thermo, USA) using thermal cycling program and primers shown in **Table 2** and **5**, respectively. Relative mRNA expression of each osteogenic marker gene was normalized to that of 18S.

Table 4. Thermal cycling program of qPCR analysis (medaka larvae)

Stage	Temperature	Hold Time
Reverse Transcription (1 cycle)	42°C	5 minutes
	95°C	10 seconds
PCR reaction (40 cycle)	95°C	5 seconds
	60°C	20 seconds
Melting Curve analysis	95°C	0 seconds
	65°C	15 seconds
	95°C	0 seconds

Table 5. Primer list for qPCR analysis (medaka larvae)

Gene	Forward Primer (5' – 3')	Backward Primer (5' – 3')
Runx2	TCAGACGCAGTCACAGA	ACTCAGGTAGGACGGATA
ALP	AGGGAAGCCGATGTTTCCTG	TCCTGCATCTTTGGCCCATT
Osx	TCTCCCCTCAGCTTCCTTAG	CTGTGTTGCAGACAGCCAGT
OPG	GCTGGTTATGTGCGTAAA	AAGAATGCTGAGAGGAA
RANKL	CTGCTTCCGCCACTACAA	GGGTTGCCAATATCCACAG
18S	CATGGCCTTCCGTGTTCCTA	CCTGCTTCACCACCTTCTTGAT

2.9. Statistical Analysis

All experiments were conducted in triplicate and results were presented as mean ± standard deviation. Except gene expression and mineralization results, which were analyzed by two-tailed Student's *t*-test, all mean values were analyzed by parametric one-way ANOVA followed by multiple comparisons using Turkey-HSD to detect significant differences at $p < 0.05$, $p < 0.01$ $p < 0.001$ (GraphPad Prism, San Diego, CA, USA).

3. Results and Discussion

3.1. Preparation of PTR-SeNPs

In this study, PTR-SeNPs was prepared according to our previously reported method [82] with some modifications, in which sodium selenite and ascorbic acid were used as the Se source and reducing agent, respectively (

Figure 8). The structure and composition PTR-SeNPs were then characterized by Nanosight NS300, HR-TEM-EDX (JEOL JEM-2100F + Horiba EX-250), and FT-IR (Nicolet™ iS™ 50) currently used in our laboratories.

During PTR-SeNPs preparation, selenite (SeO_3^{-2}) was firstly reduced to elemental selenium (Se^0) by ascorbic acid according to the following equations [97].

$$SeO_3^{-2} + 2H^+ \rightarrow H_2SeO_3$$

$$H_2SeO_3 + 2C_6H_8O_6 \rightarrow Se^0 + 2C_6H_6O_6 + 3H_2O$$

Se^0 were then aggregated to form a "Se nucleus" and continuously grew bigger. Fabricated by suitable concentration of PTR-PSP, further aggregation of "Se nucleus" was prevented within a nano range to form Se nanoparticles.

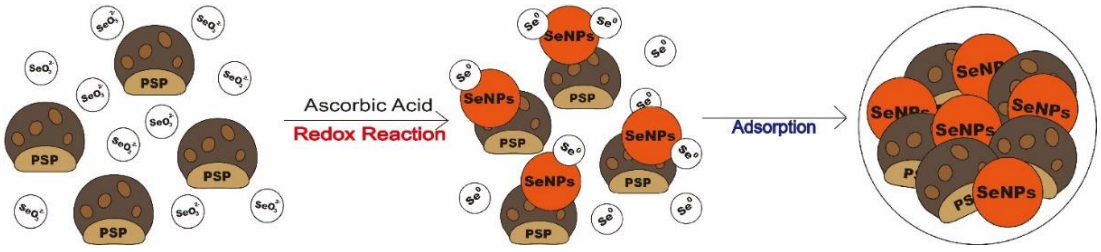

Figure 8. Schematic illustration of PTR-SeNPs preparation

3.2. Particles size and stability of PTR-SeNPs

Nanoparticle tracking analysis (NTA) measures particle size using laser to track the movement of nanoparticles within a period of time, calculating their particles size according to the rate of Brownian motion and Stokes-Einstein equation. Based on the NTA using Nanosight NS300, size distribution of the PTR-Se nanocomposite was found to has a mode of 82nm (**Figure 9A**) with an average particle size of 91.3 ± 1.53nm. As shown in **Figure 9B**, the average particle size of PTR-Se nanocomposite was highly stable without significant change in size (± 10nm) after 13 weeks' storage, suggesting its relatively high stability compared to other SeNPs prepared by using bovine serum albumin [73]. Besides, the tiny peak detected by NTA at 275nm might be due to the presence of mushroom PSP or other impurities (**Figure 9A**).

For HR-TEM, particle images are produced by differential amount of electron beam passing through the specimen and background, creating a darker areas for more electron dense regions (i.e. the particles) [98]. In this study, further characterization of PTR-SeNPs using HR-TEM (JEOL JEM-2100F; 200kV; magnification 40000×) also indicated that SeNPs itself (without mushroom PSP decoration) existed as well-dispensed spherical particles in water with an average diameter of 17.3 ± 15.0 nm (**Figure 9C & D**). It is also worth to note that majority of the resulting SeNPs was ranged from 5 to 35nm (**Figure 9D**). Among those existing international standards for "nanoparticles" shown in **Table 6**, the most widely accepted definition is that at least two dimensions of the particle are less than 100nm in size [99]. For NTA, the particles size is determined by tracking the x and y axis Brownian motion of particles, involving 2 dimension calculation of hydrodynamic diameter [100]. For ImageJ analysis of HR-TEM image, the Feret diameter measured is the longest distance of 2 parallel planes of an object with any shape [101]. In the present study, as the average particle size of PTR-SeNPs determined by both NTA and HR-TEM are less than < 100nm (**Figure 9**), PTR-SeNPs met the international standards and could be regarded as "nanoparticles".

A

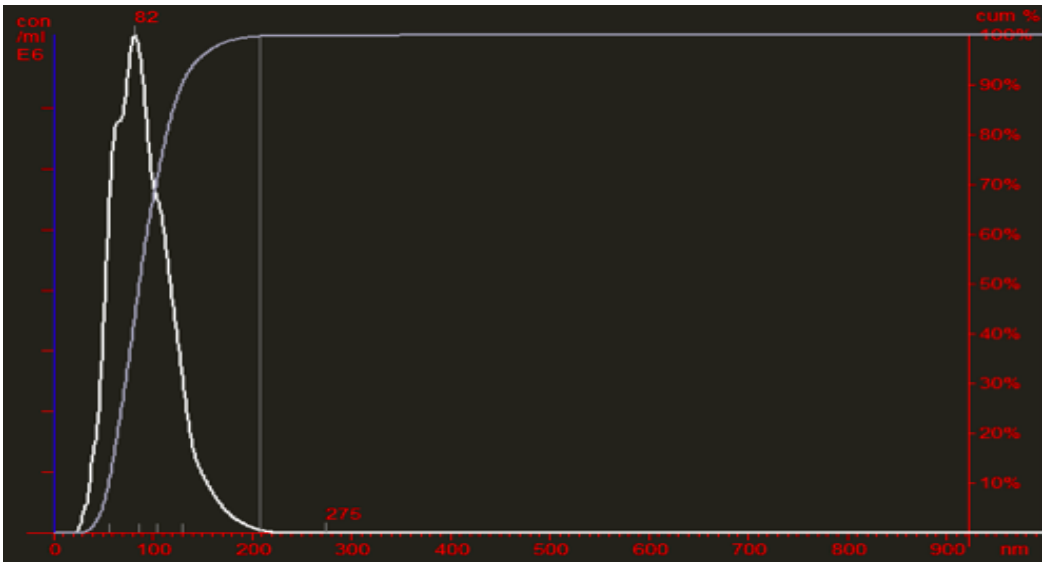
con
/ml
E6
82
cum %
100%
90%
80%
70%
60%
50%
40%
30%
20%
10%
276
0
100
200
300
400
500
600
700
800
900
nm

B

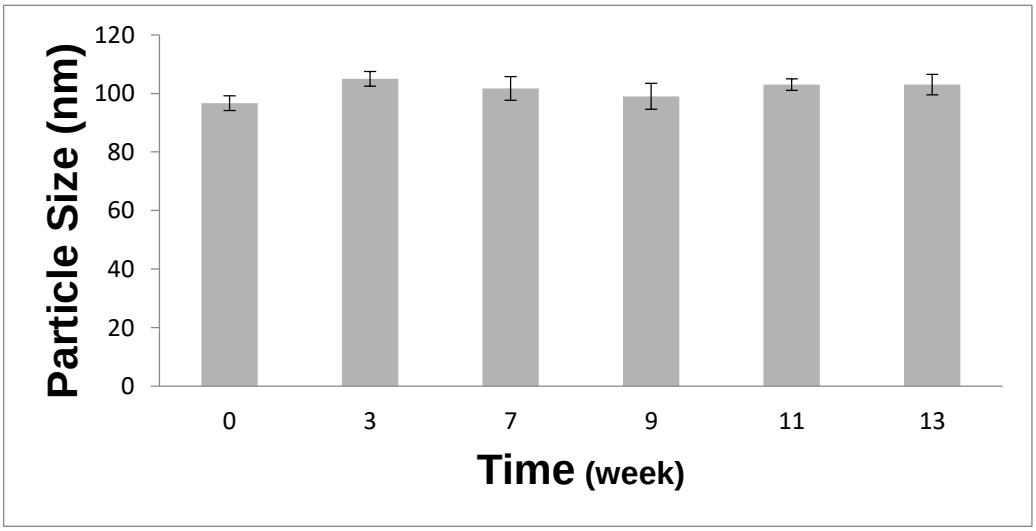
Particle Size (nm)
120
100
80
60
40
20
0
0
3
7
9
11
13
Time (week)

C

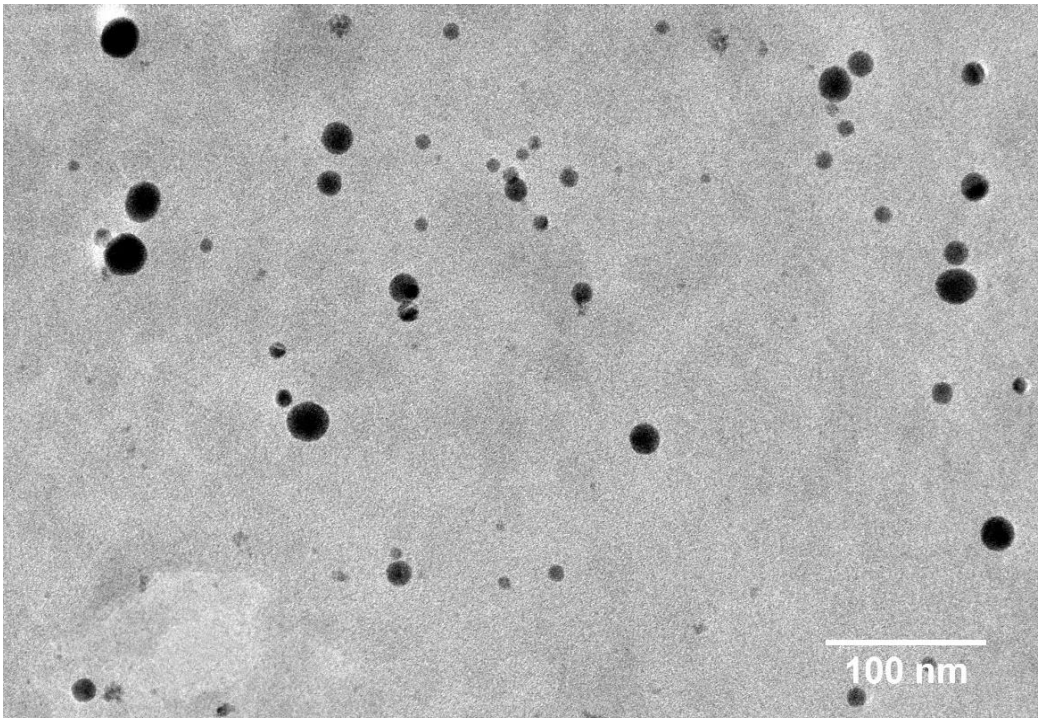
100 nm

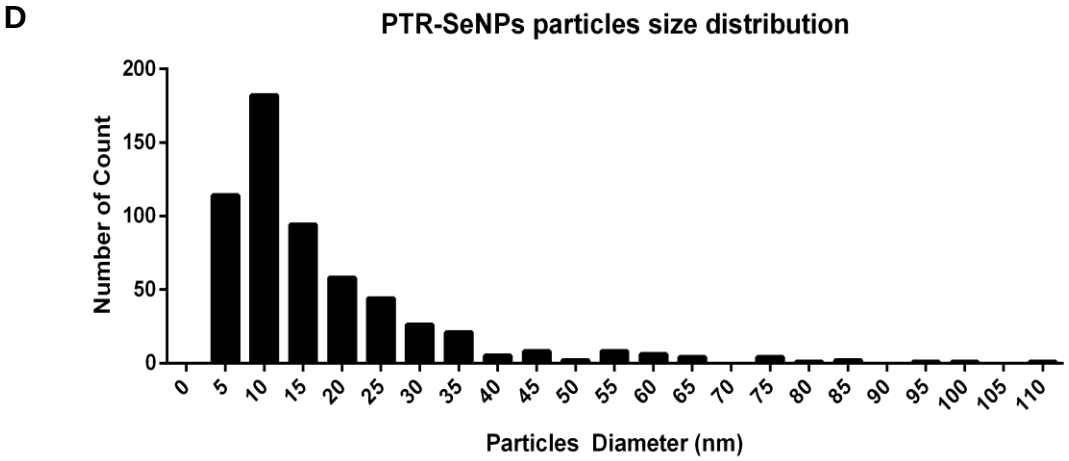

Figure 9. Particles size and stability of PTR-SeNPs.

(A) Particles size distribution of PTR-SeNPs measured by Nanosight NS300. PTR-SeNPs were diluted and its particle size distribution was determined by nanoparticle tracking analysis using Nanosight NS300. (B) Time dependent study on stability of PTR-SeNPs. PTR-SeNPs were prepared and stored at 4^{o}C for 13 weeks. Samples of PTR-SeNPs were collected every 2 weeks and their particles size was measured by Nanosight NS300. Particle size was measured 5 times for each independent determination and results were presented as mean value of three independent measurements ± S.D. (C) Representative TEM image of PTR-SeNPs. PTR-SeNPs were seeded on a hollow carbon grid and examined under HR-TEM (JEOL JEM-2100F; 200kV; magnification 40000×; scale bar: 100nm). (D) Particles size distribution of SeNPs measured by HR-TEM. HR-TEM images obtained were analyzed with ImageJ to calculate particle size of SeNPs. Results were based on three independent measurements (600 particles/ measurement).

Table 6. Existing international standards for nanoparticles

Standard	Nanoparticle
International Organization for Standardization (ISO)	A particle spanning 1 – 100nm (diameter)
American Society of Testing Materials (ASTM)	An ultrafine particle whose length in 2 or 3 places is 1 – 100nm
National Institute of Occupational Safety and Health (NIOSH)	A particle with diameter between 1 and 100nm, or a fiber spanning the range 1 – 100nm
British Standards Institution (BSI)	All the fields or diameters are in the nanoscale range

3.3. Characterization of PTR-SeNPs using HR-TEM-EDX and FT-IR

For individual PTR-SeNP, in addition to having clear lattice fringes/d-spacing (0.33nm; **Figure 10A**), the SAED pattern of PTR-SeNPs exhibited diffuse rings constructed with white dots (**Figure 10B**), collectively indicating that the nanoparticle possessed a polycrystalline structure [98]. Besides, PTR-SeNPs shared a very similar 6-ring SAED pattern to that of Se-nanocrystallites in SiO_2, suggesting a cubic crystal structure as previously reported [102]. Further investigation on its elemental composition by EDX analysis also showed that PTR-SeNPs contained high level of Se (81.2%; **Figure 10C**), indicating a successfully fabrication of SeNPs using mushroom PSP. Table 7 showed that protein (50.3%) and polysaccharide (48.8%) were the major components of PTR-PSP, suggesting a rich source of hydroxyl (–OH–) and imino (–CO–NH–) groups. In this study, the chemical binding of mushroom PSP to the surface of SeNPs was further investigated by FT-IR analysis. As shown in **Figure 10D**, the absorption peaks at 1538.7 and 3390 – 3400cm^{-1} in the IR spectrum of PTR-PSP corresponded to the secondary imino (–CO–NH–) groups of its proteins and the stretching vibrations of hydroxyl (–OH–) groups of its polysaccharides. Interestingly, PTR-PSP shared very a similar FT-IR spectrum to that of PTR-SeNPs, indicating that PTR-PSP formed part of the PTR-SeNPs nanocomposite. Nevertheless, both absorption peaks of hydroxyl groups and imino groups shifted from 1538.7 to 1537.2 and from 3397.23 to 3393.47, respectively, indicating the occurrence of interaction

between the hydroxyl groups and imino groups of PTR-PSP and the Se atoms as previously reported [82]. These results suggest that the SeNPs were capped by mushroom PSP mainly through the formation of Se-O and Se-N bonds, leading to a stable spherical structure of SeNPs.

A

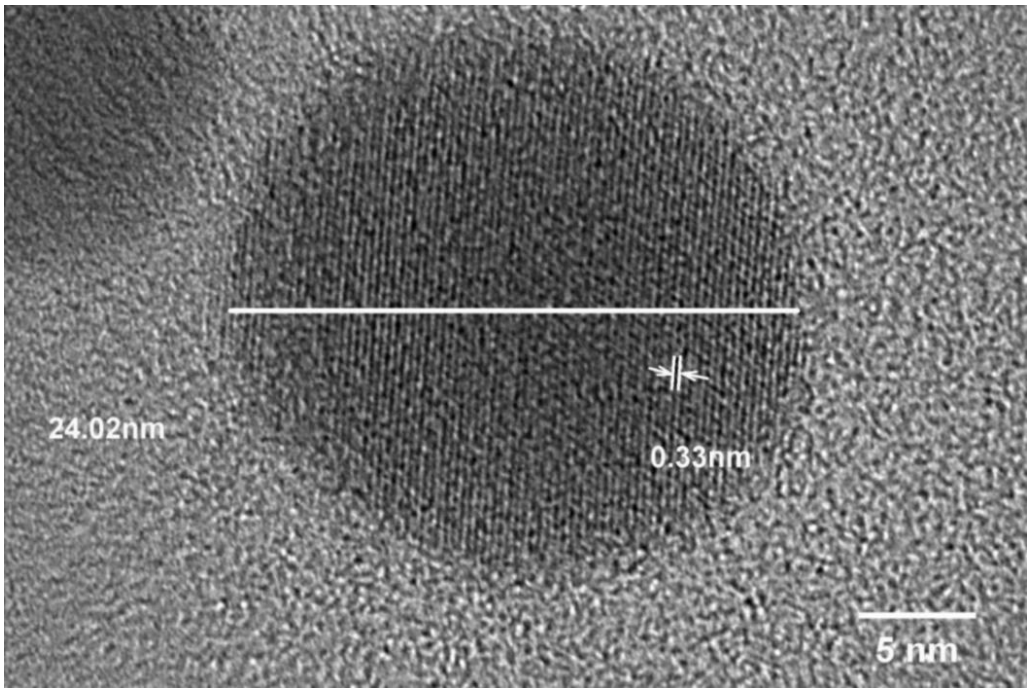
24.02nm
0.33nm
5 nm

B

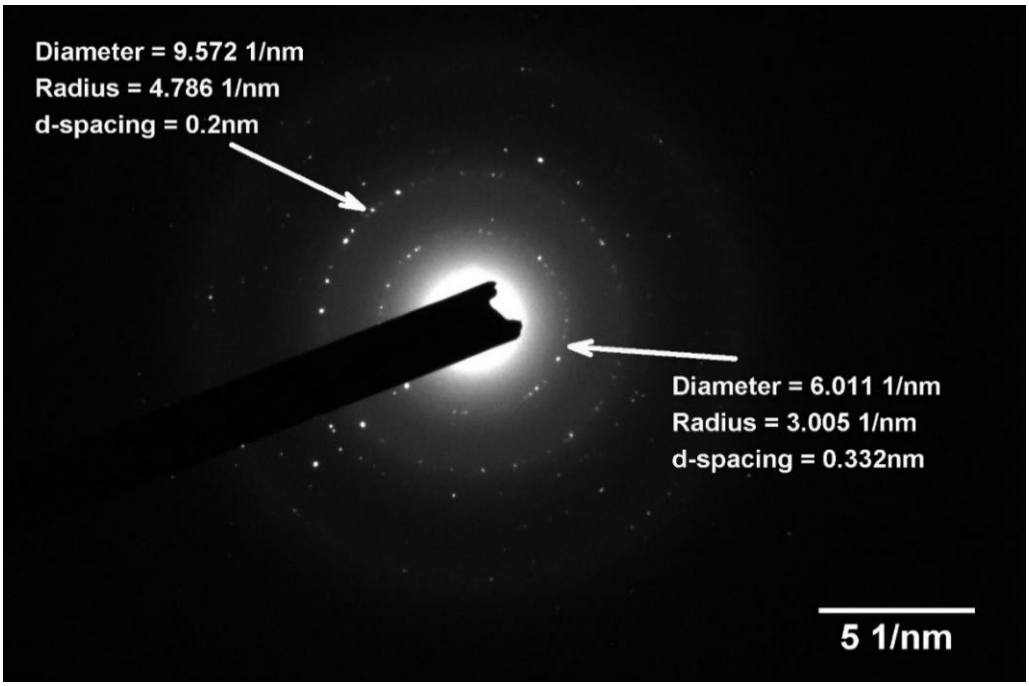
Diameter = 9.572 1/nm
Radius = 4.786 1/nm
d-spacing = 0.2nm
Diameter = 6.011 1/nm
Radius = 3.005 1/nm
d-spacing = 0.332nm
5 1/nm

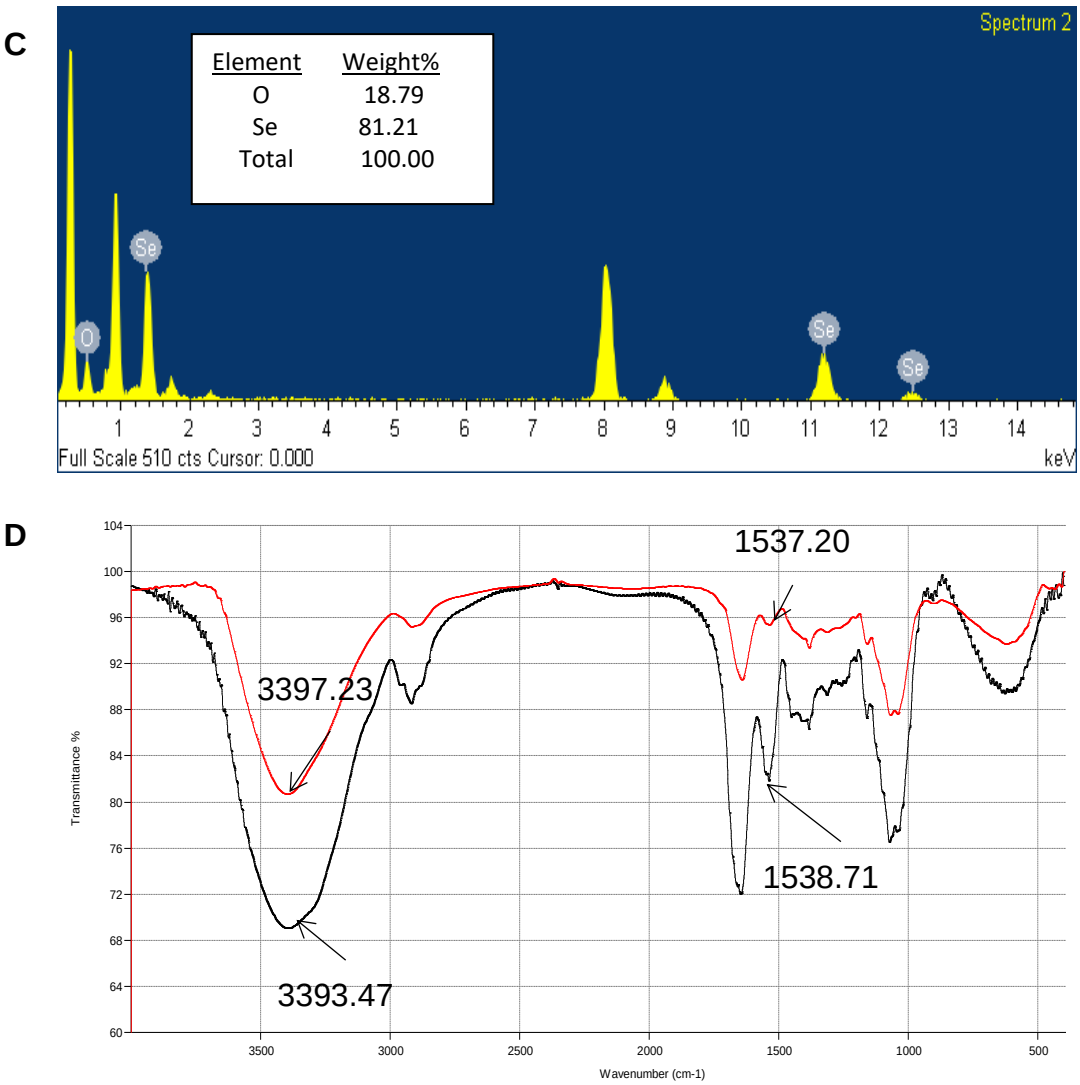

Figure 10. Representative HR-TEM image of (A) lattice fringes and (B) corresponding selected area electron diffraction (SAED) pattern of PTR-SeNPs. PTR-SeNPs was seeded on a hollow carbon grid and examined under HR-TEM (20keV; 150000×). Lattice fringes as well as diameter, radius and d-spacing of diffraction rings were measured using ImageJ. (C) Representative EDX analysis of PTR-SeNPs. (D) FT-IR analysis of PTR-SeNPs and PTR-PSP. Freeze-dried PTR-SeNPs and PTR-PSP were mixed with KBr to form sample discs followed by analysis using Nicolet™ iS™ 50 FT-IR Spectrometer.

Table 7. Composition of PTR-PSP

Composition	Percentage
Polysaccharide	48.8%
Protein	50.3%

3.4. Direct Effects of PTR-SeNPs on Bone Formation Using MC3T3 E-1 Cells

3.4.1. Cell proliferation

In general, PTR-SeNPs was found to exhibit a significant dose-dependent proliferation effect (range from 1.33 – 1.73 folds) on the MC3T3-E1 cells for 24, 48 and 72 hours with the most effect dosage of 10μM (**Figure 11A-C)**. In addition to 10μM of sodium selenite (common food source of inorganic Se), we further compared the proliferation effect of PTR-SeNPs (10μM) and PTR-PSP alone at concentration used for preparing 10μM of PTR-SeNPs (i.e. 6μg/mL) in order to investigate whether mushroom PSP decoration would contribute the proliferation effect of PTR-SeNPs on MC3T3-E1 cells. Interestingly, except for 48-hour treatment, PTR-PSP had no effect on the proliferation of MC3T3-E1 cells, and sodium selenite (10μM) was even found to significantly inhibit the growth of MC3T3-E1 cells for all time intervals (**Figure 12A-C**). In contrast, the significantly highest proliferation effect of PTR-SeNPs on the MC3T3-E1 cells (**Figure 12A-C**) suggested that SeNPs itself, instead of PSP, was mainly responsible for the proliferation effect of whole PTR-Se nanocomposite, having relatively lower toxicity than that of sodium selenite under the same dosage. Besides, it is worth noting that, compared with the effective dosage (640μM) of other SeNPs on bone cell proliferation [103], PTR-SeNP exhibited strong proliferation effect on bone cells with remarkable low concentration (10μM only).

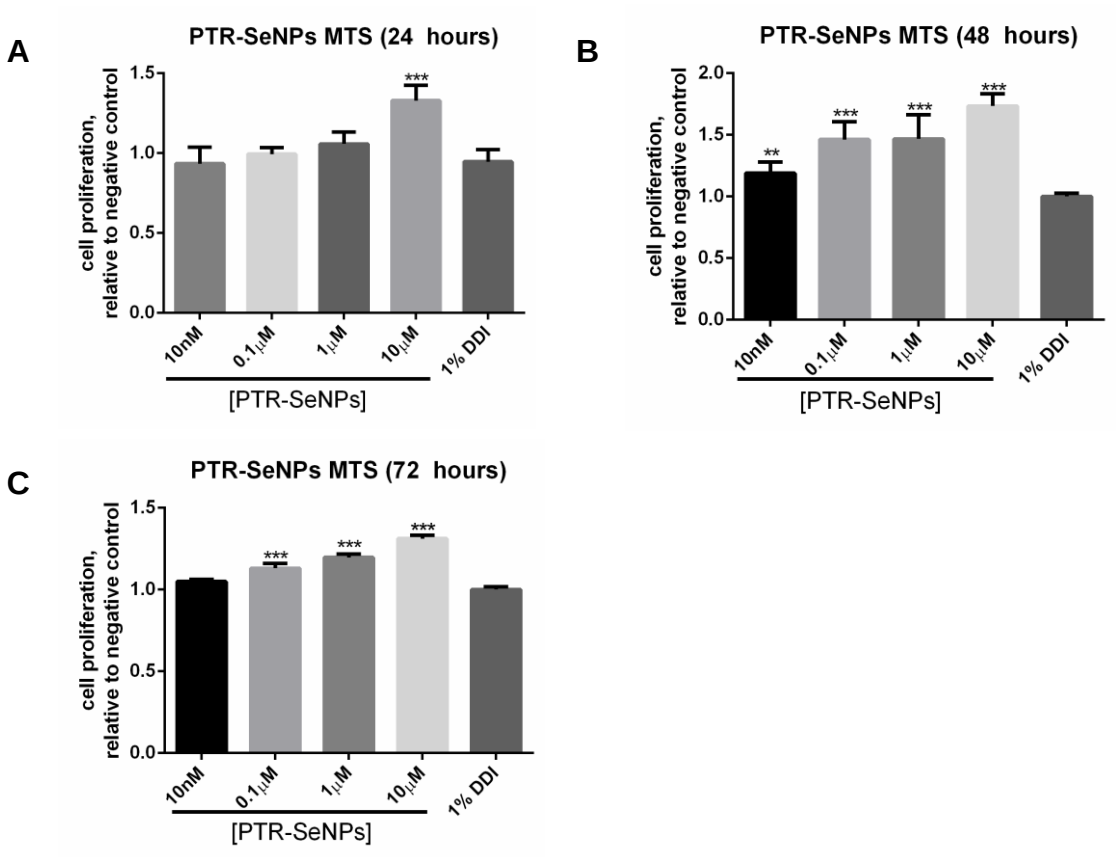

Figure 11. Dose and time dependent study of the proliferation effect of PTR-SeNPs on MC3T3-E1 cells. Cells were treated with different concentrations of PTR-SeNPs (10nM - 10μM) in normal medium for (A) 24 (B) 48 and (C) 72 hours. Cell proliferation was determined by MTS assay and results were normalized and compared with that of negative control group (1% deionized water; 1% DDI). Results are mean values of three determinations ± SEM. Means with "***" are significantly different ($p < 0.001$, one-way ANOVA).

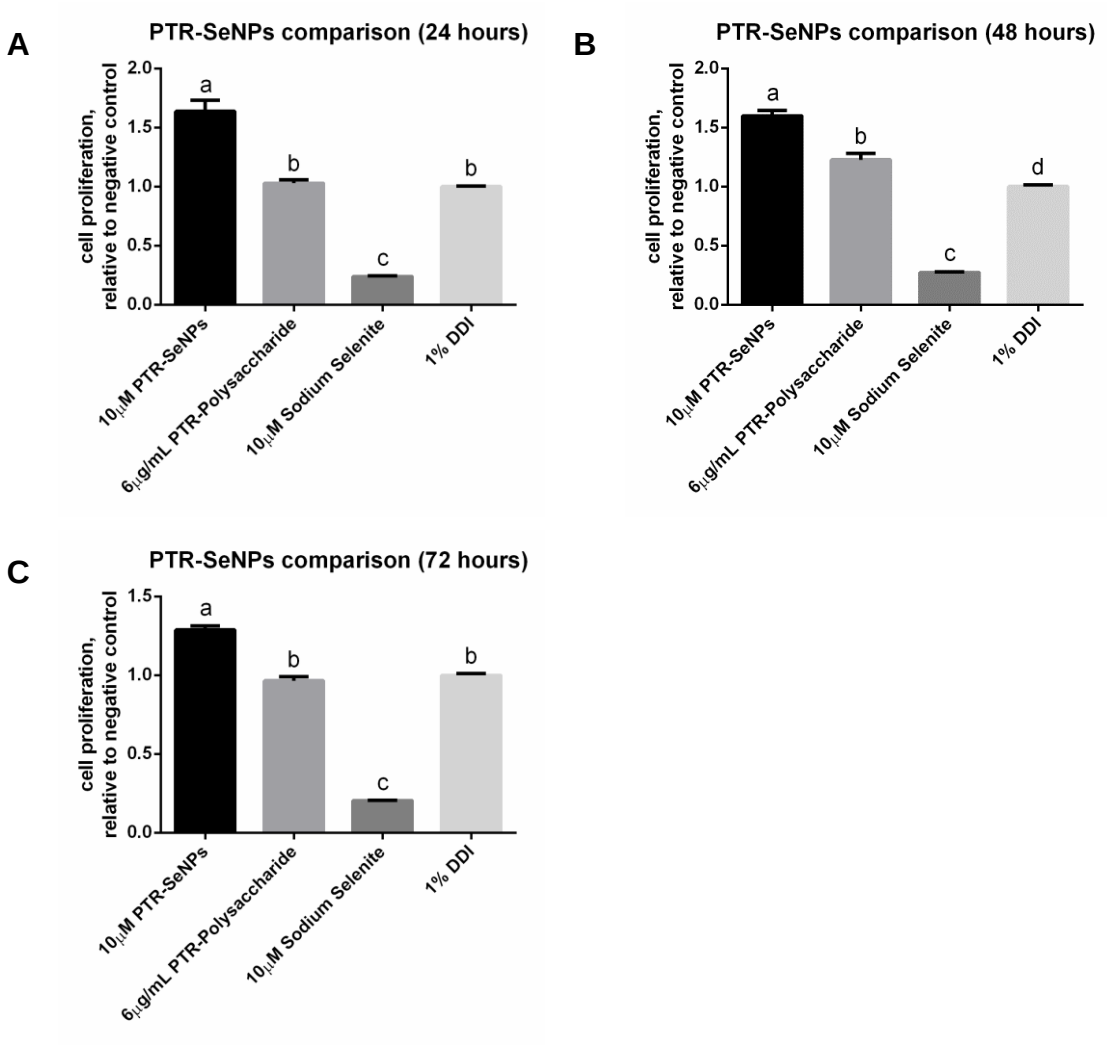

Figure 12. Time-dependent study of proliferation effect of PTR-SeNPs, PTR-PSP and sodium selenite on MC3T3-E1 cells. Cells were treated with PTR-SeNPs (10μM), PTR-PSP (6μg/mL) and Na_2SeO_3 (10μM) in normal medium for (A) 24, (B) 48 and (C) 72 hours. Cell proliferation was determined by MTS assay and results were normalized and compared with negative control group (1% deionized water; 1% DDI). Results are mean values of three determinations ± SEM. Means with letters (a-d) are significantly different ($p < 0.05$, one-way ANOVA).

3.4.2. Osteoblastic differentiation and bone mineral formation

ALP is a phosphor-hydrolytic enzyme that plays a major role in bone formation, regarding as a phenotypic marker for osteoblasts during differentiation. As shown in **Figure 13A** and **15A**, PTR-SeNPs (10μM) markedly induced the osteoblastic differentiation of MC3T3-E1 cells after a 7-day treatment as evidenced by a significant increase in ALP activity (1.36 ± 0.10 folds) and up-regulation of ALP gene expression (2.09-folds). The ALP containing MC3T3-E1 cells pre-treated with 10μM of PTR-SeNPs (purple-blue area) were further visualized by ALP staining (**Figure 13B**).

Mineralization is the final stage of osteogenesis and osteocalcin (OCN) which expresses in differentiating cells of intermediate and mature nodules, is a specific marker gene for mineralization. As shown in **Figure 14A&B**, PTR-SeNPs (10μM) significantly promoted the bone nodule formation in MC3T3-E1 cells as visualized by both Von Kossa (20 folds) or alizarin red S staining (3 folds) followed by semi-quantification of corresponding calcium deposition. Further investigation on the gene expression of OCN also indicated that PTR-SeNPs (10μM) could significantly up-regulate this mineralization maker gene for 9.69 folds (**Figure 15B**), demonstrating its strong stimulating effect on bone mineralization.

Runx2 and osterix (Osx) are the two main osteoblastic transcription factors in osteogenesis [104, 105]. Activation of Runx2 has been found to upregulate several osteoblast-specific genes (such as OCN), promoting bone formation in both cell and animal models [106-108]. Similarly, Osx is another critical transcriptional factor in osteoblast differentiation and bone formation previously identified in a Osx-null mutant mice study [56]. As shown in **Figure 15B & C**, the gene expression of both Runx2 (2.11 folds) and Osx (1.87 folds) in MC3T3-E1 cells pre-treated with 10μM of PTR-SeNPs were significantly up-regulated, indicating that PTR-SeNPs (10μM) enhanced the osteoblastic differentiation and bone formation in MC3T3-E1 cells mediated by these two transcription factors.

Bone remodeling is a lifelong process of regulating "new bone formation" and "old bone resorption". These two sub-processes are governed by specialized cell types named "osteoblast" as well as "osteoclast" and an imbalance of which results in metabolic bone diseases like osteoporosis [31]. OPG and RANKL are bone remodeling markers secreted by osteoblasts for inhibiting and activating osteoclasts, respectively [109, 110]. Thus, OPG/RANKL ratio is a widely used parameter to figure out the possible interaction between osteoblasts and osteoclasts. Interestingly, our study discovered that PTR-SeNPs (10μM) significantly up-regulate the expression of both OPG and RANKL

to different extent, however, resulting in significant increase of the OPG/RANKL ratio (2.11 ± 0.33 folds; **Figure 15D**). In addition to direct promoting osteoblastogenesis, this finding suggested that PTR-SeNPs (10μM) also exhibited indirect inhibition effect on osteoclastogenesis.

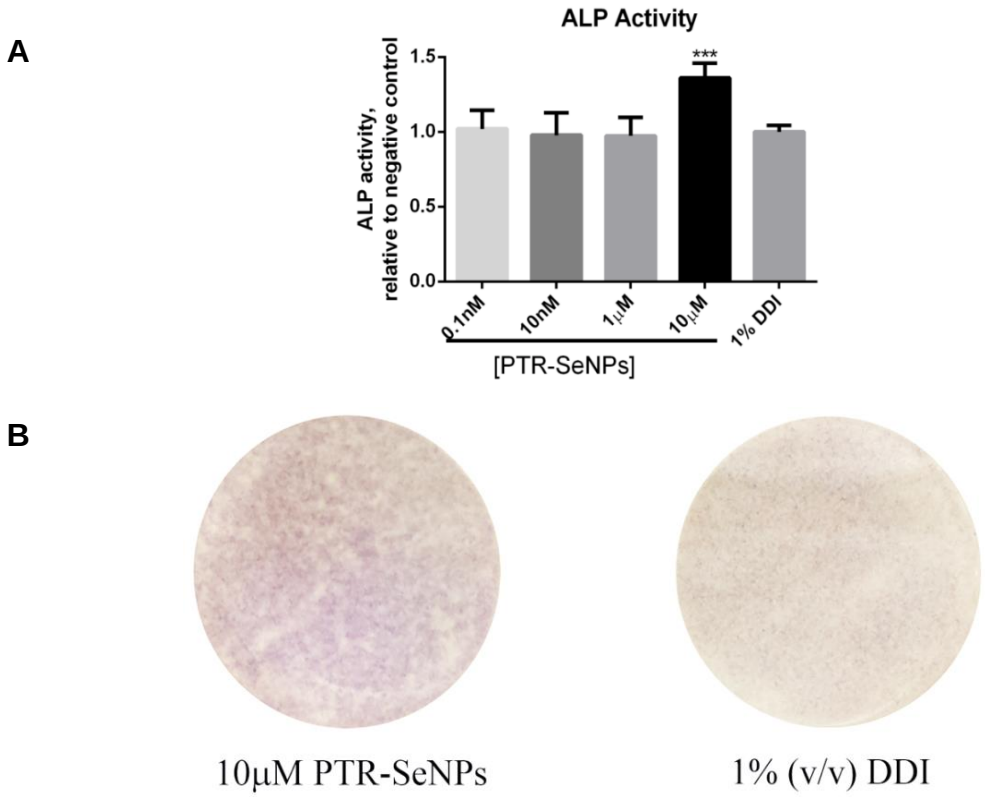

Figure 13. PTR-SeNPs induced osteoblastic differentiation in MC3T3-E1 cells. (A) ALP activity in MC3T3 cells pre-treated with different concentrations of PTR-SeNPs (0.1nM-10μM) in osteogenic medium for 7 days was determined by spectrophotometry at 410nm and normalized relative to the total cellular protein content. Normalized results were compared with that of the negative control group (1% deionized water; 1%DDI). (B) ALP containing MC3T3-E1 cells pre-treated with 10μM of PTR-SeNPs or 1% (v/v) DDI were visualized by ALP staining. Results are mean values of three determinations ± SEM. Means with "***" are significantly different ($p < 0.001$, one-way ANOVA or Student's *t* test).

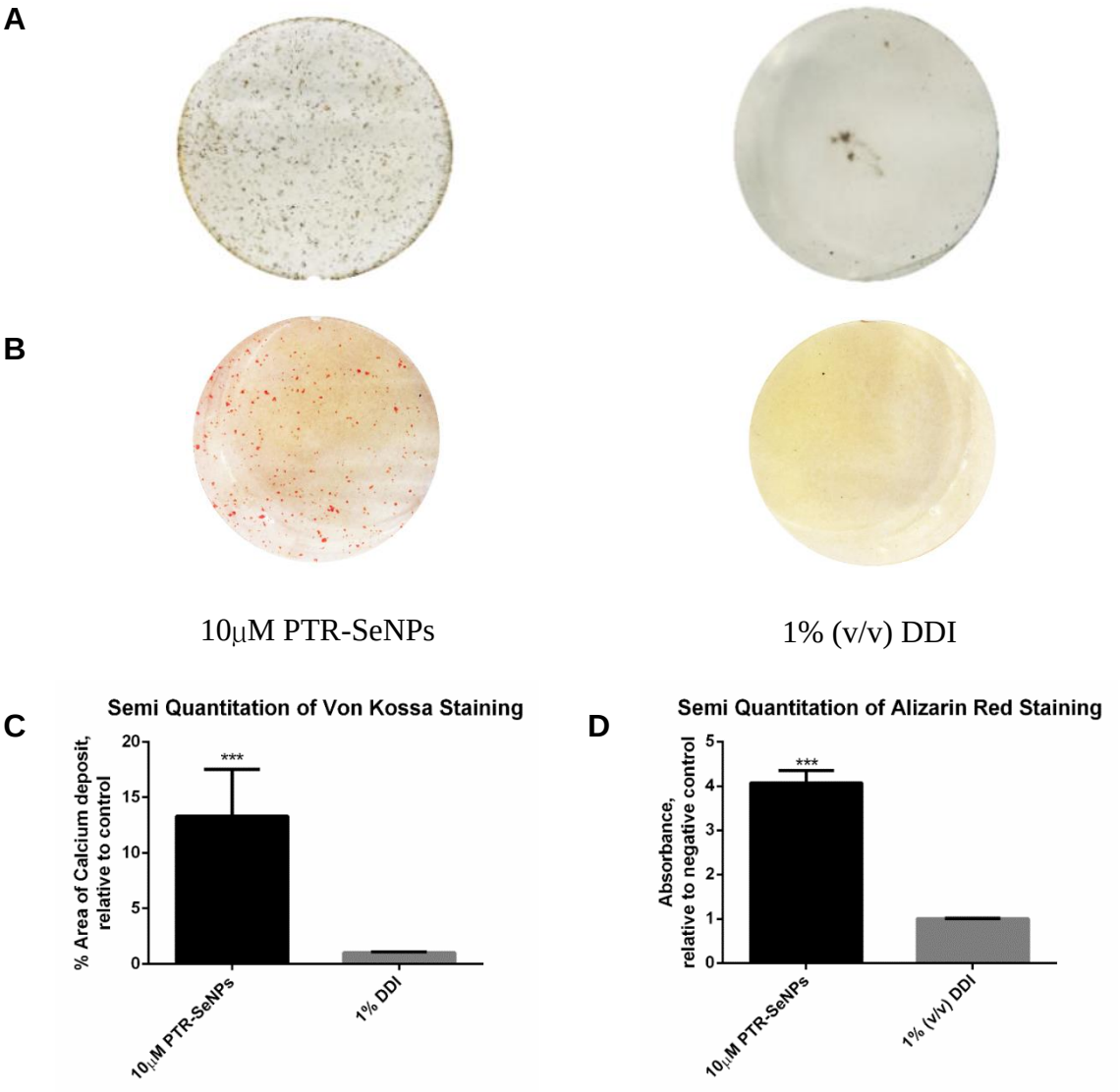

Figure 14. PTR-SeNPs simulated bone mineral formation in MC3T3-E1 cells. Bone nodules formation in MC3T3 cells pre-treated with 10μM of PTR-SeNPs in osteogenic medium for 16 days was visualized by (A) Von Kossa staining and (B) Alizarin Red S staining. (C) Semi-quantification of Von Kossa staining was obtained by ImageJ. (D) Semi-quantification of Alizarin Red S staining was determined by spectrophotometry. Results are mean values of three determinations ± SEM. Means with "***" are significantly different ($p < 0.001$; one-way ANOVA or Student's *t* test).

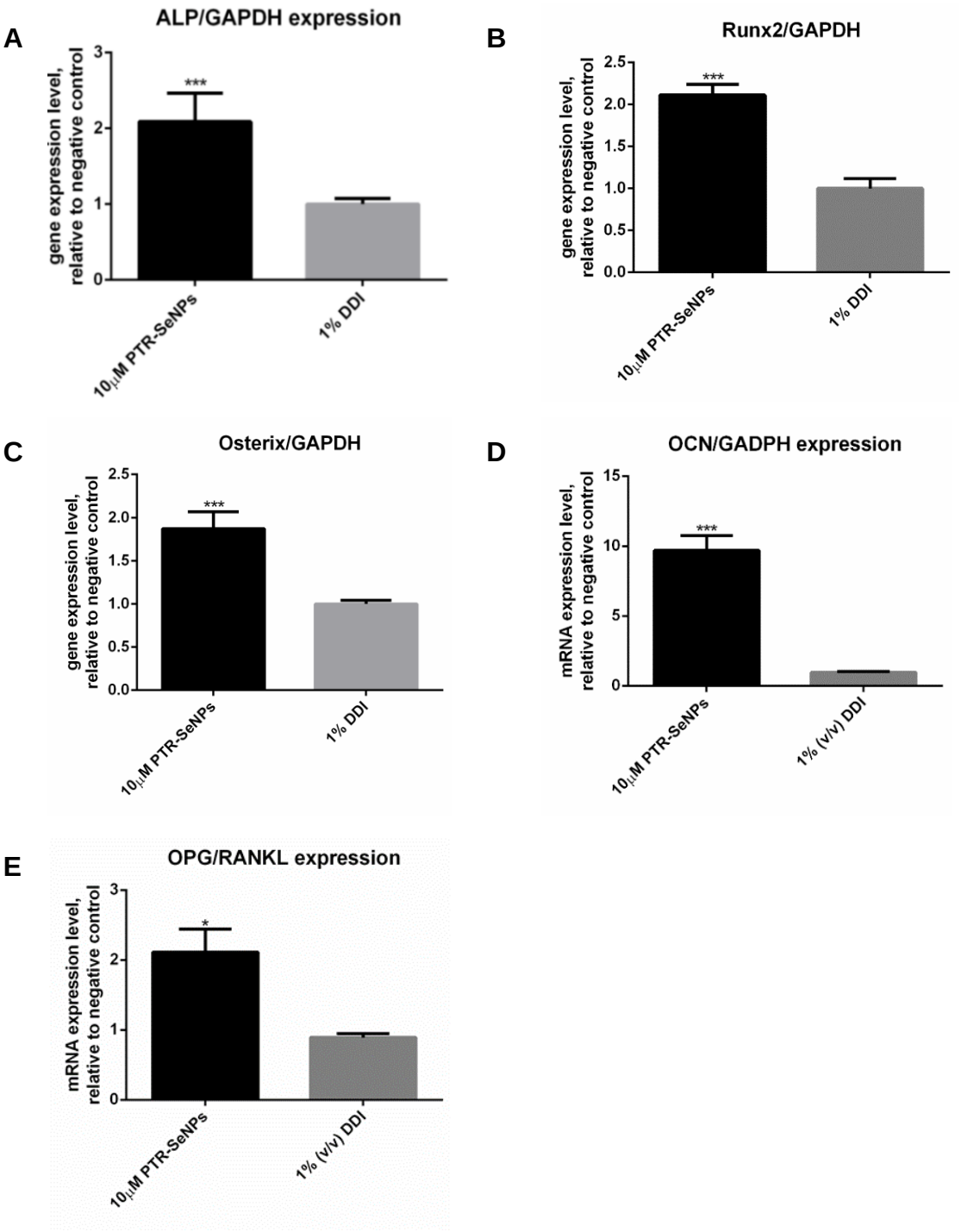

Figure 15. PTR-SeNPs upregulated the major osteogenic markers in MC3T3-E1 cells during osteoblastic differentiation and mineralization. Gene expression of (A) ALP, (B) Runx2, (C) Osx, (D) OCN and (E) OPG/RANKL in MC3T3-E1 cells pre-treated with 10μM of PTR-SeNPs or 1% (v/v) DDI for 3 (Runx2), 7 (ALP & Osx), 11

(OPG/RANKL) and 16 days (OCN) was quantified by qPCR analysis and normalized to that of GAPDH. Results are mean values of three determinations ± SEM. Means with "*" or "***" are significantly different ($p < 0.05$ and $p < 0.001$; Student's t test).

3.5. BMP-2 Signaling Cascades Modulated by PTR-SeNPs in the MC3T3 E-1 Cells During Osteoblast Differentiation

Substantial evidences have demonstrated that BMP-2 signaling via Smad-dependent and/or Smad-independent pathway(s) is one the most important signaling cascades in regulating osteoblastogenesis [36-38]. In Smad-dependent pathway, upon cell surface ligand binding, BMP-2 forms a hetero-tetrameric receptor complex with the dimers of both type II and type I transmembrane serine/threonine kinases, triggering phosphorylation of Smad1/5/8 in the cytoplasm. Phosphorylated Smad1/5/8 then forms a trimetric complex with Smad4 followed by translocation to nucleus, where they regulate the transcription of target genes for osteoblast differentiation. In particular, homeobox gene Dlx5, which is an upstream target of both BMP-2/Smad dependent and BMP-2/Smad independent pathways, plays a pivotal role in stimulating the downstream transcription factors such as Runx2 and Osx [34]. MAPKs (including p38, ERK and JNK) signaling, which are upstream regulators of Dlx5 in the BMP-2/Smad independent pathway, has been found to play important role in osteoblast differentiation, regulating the ALP, Runx2 and OCN expressions [34]. Interestingly, we discovered that PTR-SeNPs (10μM) not only significantly upregulated the gene expression of BMP-2 (1.64 ± 0.24 folds) and Dxl5 (1.54 ± 0.06 folds) but also markedly increased the protein phosphorylation of Smad1/5/8 (1.31 ± 0.06 folds) and

all MAPKs such as p38 (2.86 ± 0.58 folds), ERK (3.67 ± 1.48 folds) and JNK (1.36 ± 0.07 folds) (**Figure 19)**. The involvement of BMP-2/Smad dependent pathway in SeNPs (functionalized by ruthenium and citrate) mediated osteoblast differentiation has been reported recently [84]. Surprisingly, our findings suggest that PTR-SeNPs could trigger both BMP-2/Smad-dependent and Smad-independent pathways in the MC3T3-E1 cells during osteoblast differentiation. The proposed BMP-2 signaling cascades modulated by PTR-SeNPs in the MC3T3-E1 cells during osteoblast differentiation are shown in **Figure 19**. Nevertheless, after cellular internalization, the specific role of PTR-SeNPs in regulating osteoblastogenesis of MC3T3 E-1 cells via BMP-2/Smad dependent and independent pathways is not clear at this stage and will be further discussed later.

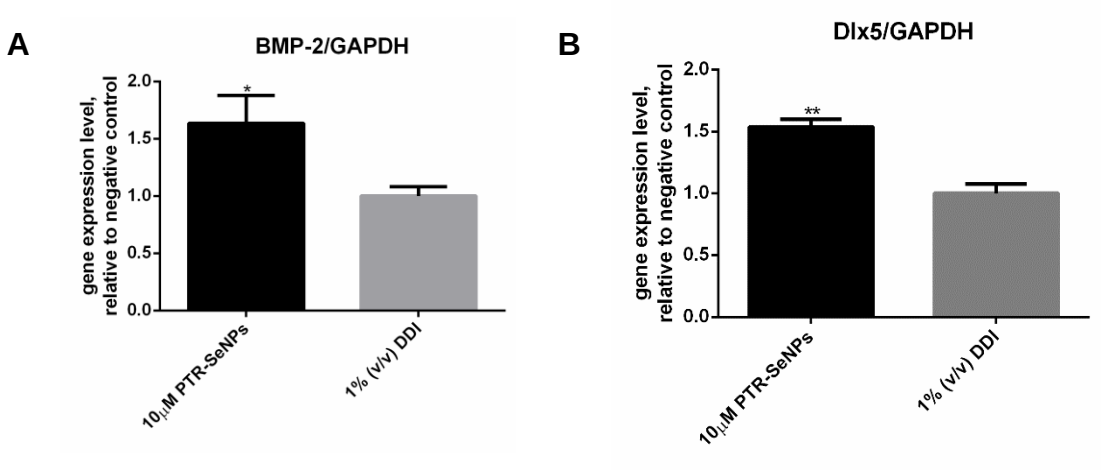

Figure 16. PTR-SeNPs upregulated the BMP-2 and Dlx5 in MC3T3-E1 cells during osteoblastic differentiation. Gene expression of (A) BMP-2 and (B) Dlx5 in MC3T3-E1 cells pre-treated with 10μM of PTR-SeNPs or 1% (v/v) DDI for 3 (BMP-2) and 7 days (Dlx5) was quantified by qPCR analysis and normalized to that of GAPDH. Results are mean values of three determinations ± SEM. Means with "*" and "**" are significantly different ($p < 0.05$ and $p < 0.01$; Student's *t* test)

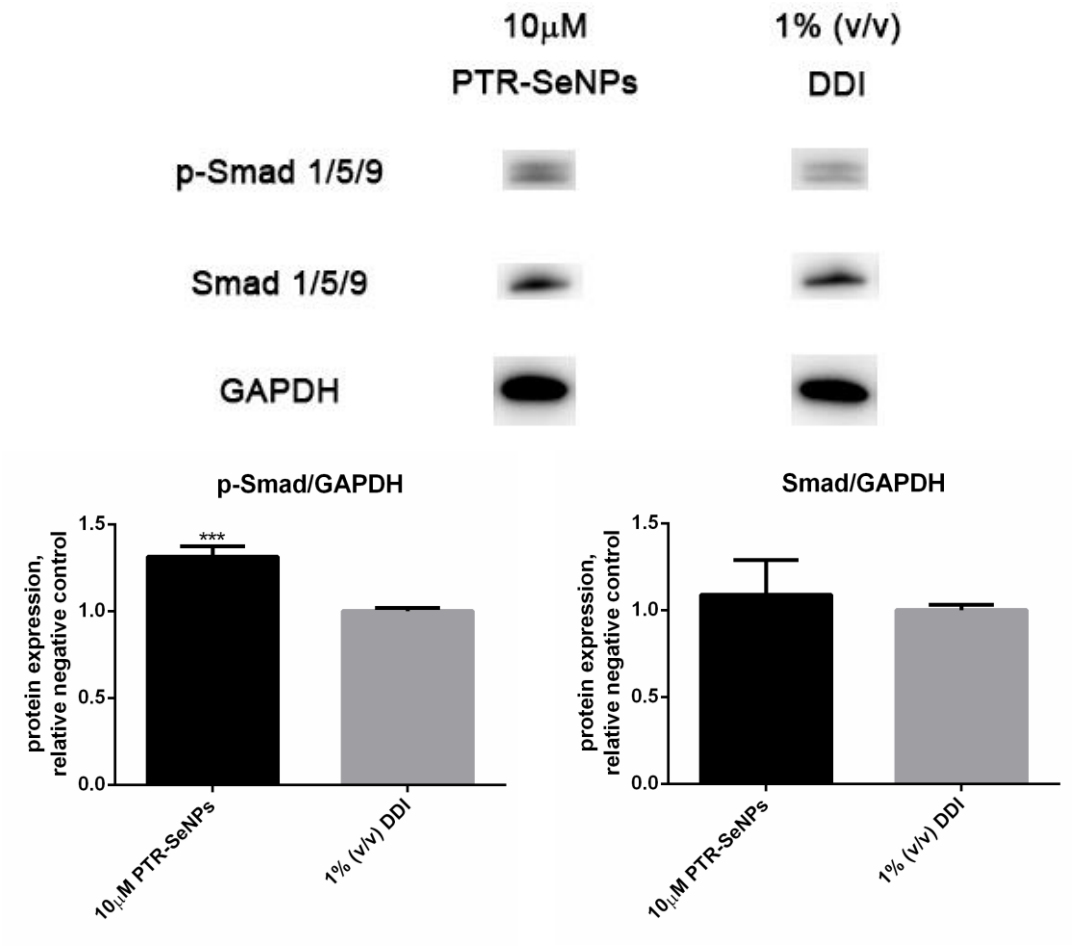

Figure 17. PTR-SeNPs induced the BMP-2/Smad dependent pathway in MC3T3-E1 cells. Protein expression and phosphorylation of Smad1/5/9 in MC3T3-E1 cells pre-treated with 10μM of PTR-SeNPs or 1% (v/v) DDI for 4 days was quantified by Western blot analysis and normalized to that of GAPDH. Semi-quantification of images was obtained by ImageJ. Results are mean values of three determinations ± SEM. Means with "***" are significantly different ($p < 0.001$; Student's *t* test).

A

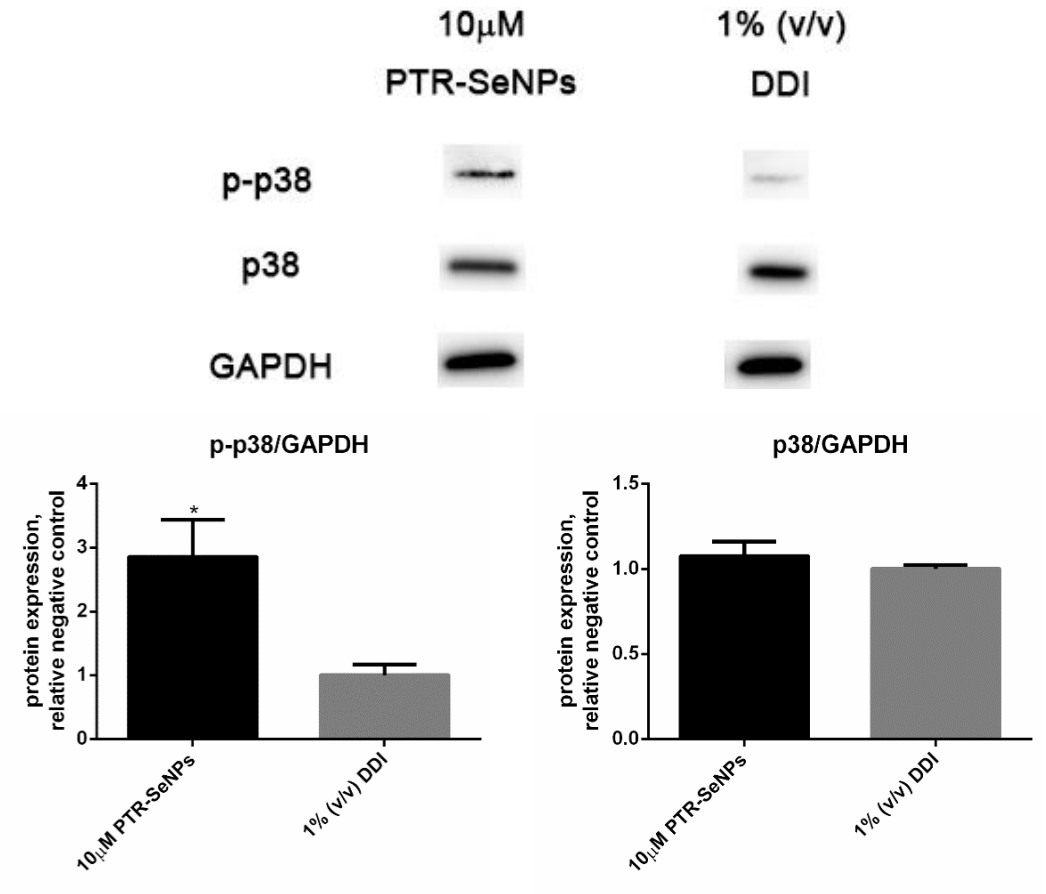
10μM
PTR-SeNPs
1% (v/v)
DDI
p-p38
p38
GAPDH
p-p38/GAPDH
protein expression, relative negative control
*
10μM PTR-SeNPs
1% (v/v) DDI
p38/GAPDH
protein expression, relative negative control
10μM PTR-SeNPs
1% (v/v) DDI

B

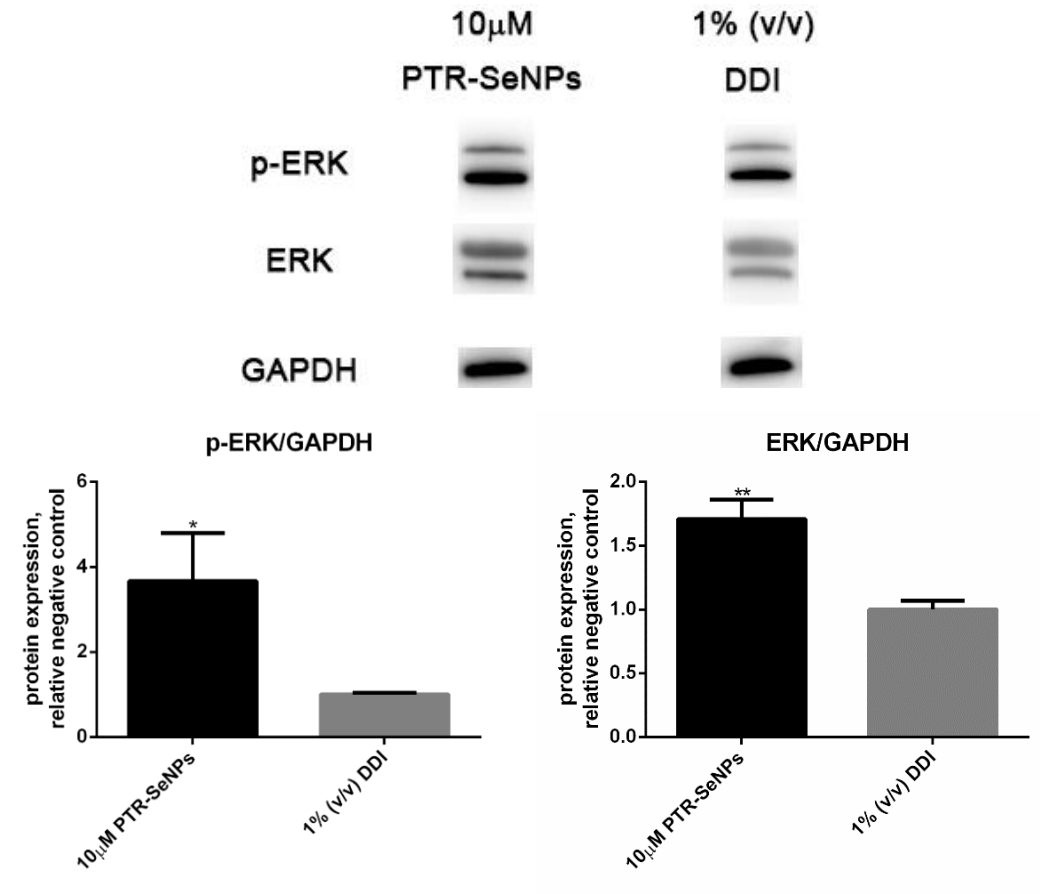
10μM
PTR-SeNPs
1% (v/v)
DDI
p-ERK
ERK
GAPDH
p-ERK/GAPDH
protein expression, relative negative control
*
10μM PTR-SeNPs
1% (v/v) DDI
ERK/GAPDH
protein expression, relative negative control
**
10μM PTR-SeNPs
1% (v/v) DDI

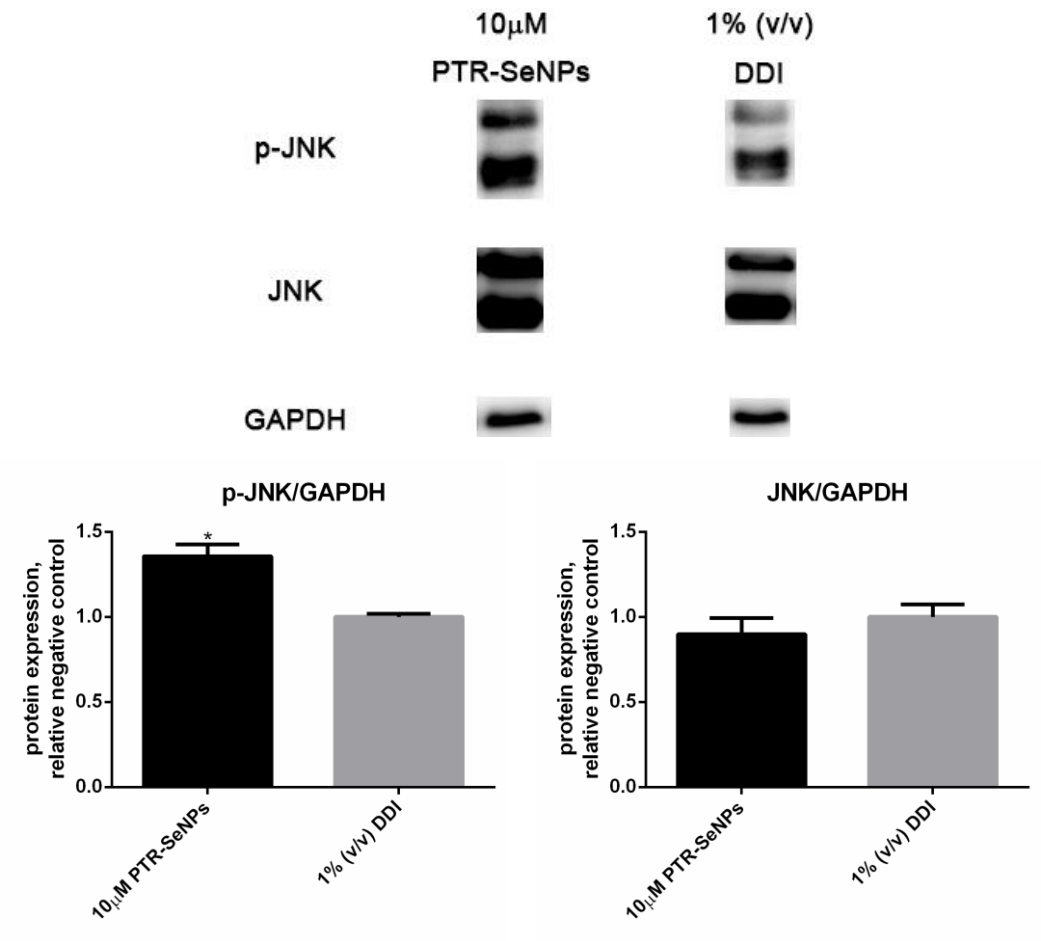

Figure 18. PTR-SeNPs induced the BMP-2/Smad independent pathway in MC3T3-E1 cells. Protein expression and phosphorylation of (A) p38, (B) ERK and (C) JNK in MC3T3-E1 cells pre-treated with 10μM of PTR-SeNPs or 1% (v/v) DDI for 4 days was quantified by Western blot analysis and normalized to that of GAPDH. Semi-quantification of images was obtained by ImageJ. Results are mean values of three determinations ± SEM. Means with "*" and "**" are significantly different ($p < 0.05$ and $p < 0.001$; Student's t test).

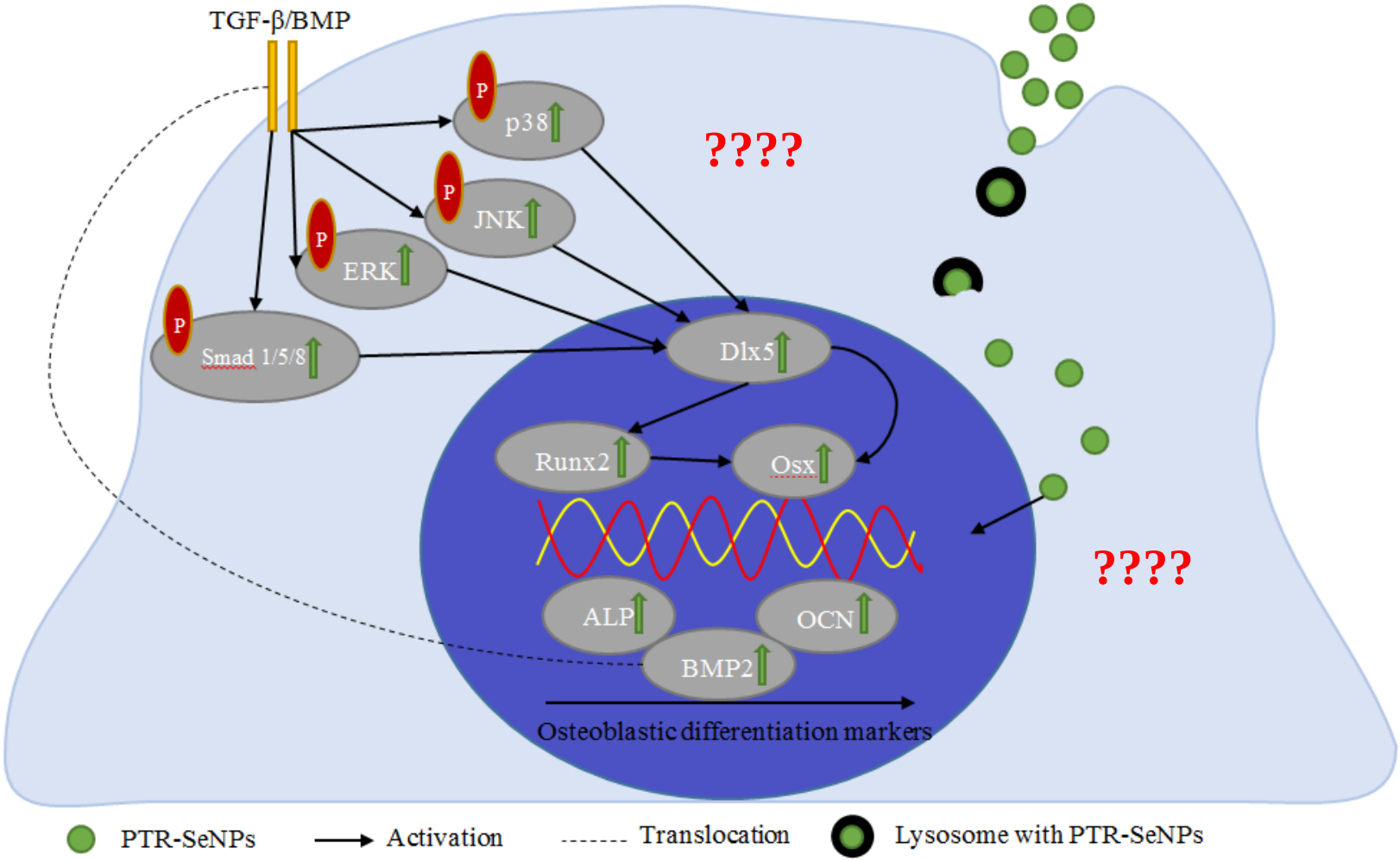

Figure 19. Proposed BMP-2 signaling mediated by PTR-SeNPs in MC3T3-E1 cells during osteoblast differentiation

3.6. Cellular Uptake Behavior of PTR-SeNPs by the MC3T3-E1 Cells

Endocytosis has been widely reported as the major cellular uptake mechanism for nanoparticles [85]. Our preliminary study found that after cellular internalization, coumarin-6 labelled PTR-SeNPs (120μM) co-localized with lysosomes in the MCF-7 human breast carcinoma cells around 10 min [82]. Similarly, as shown in **Figure 20**, the overlay of the blue (nucleus), green (PTR-SeNPs) and red (lysosomes) fluorescence clearly indicated the co-localization of PTR-SeNPs (10μM) and lysosomes in the MC3T3-E1 cells as early as 5 min, suggesting that lysosome is the main target organelle of PTR-SeNPs. Subsequently, some PTR-SeNPs were found to escape from lysosomes and released into cytosol from 6 min onwards. It is the first study of its kind to report the intracellular localization of SeNPs by MC3T3-E1 cells via endocytosis.

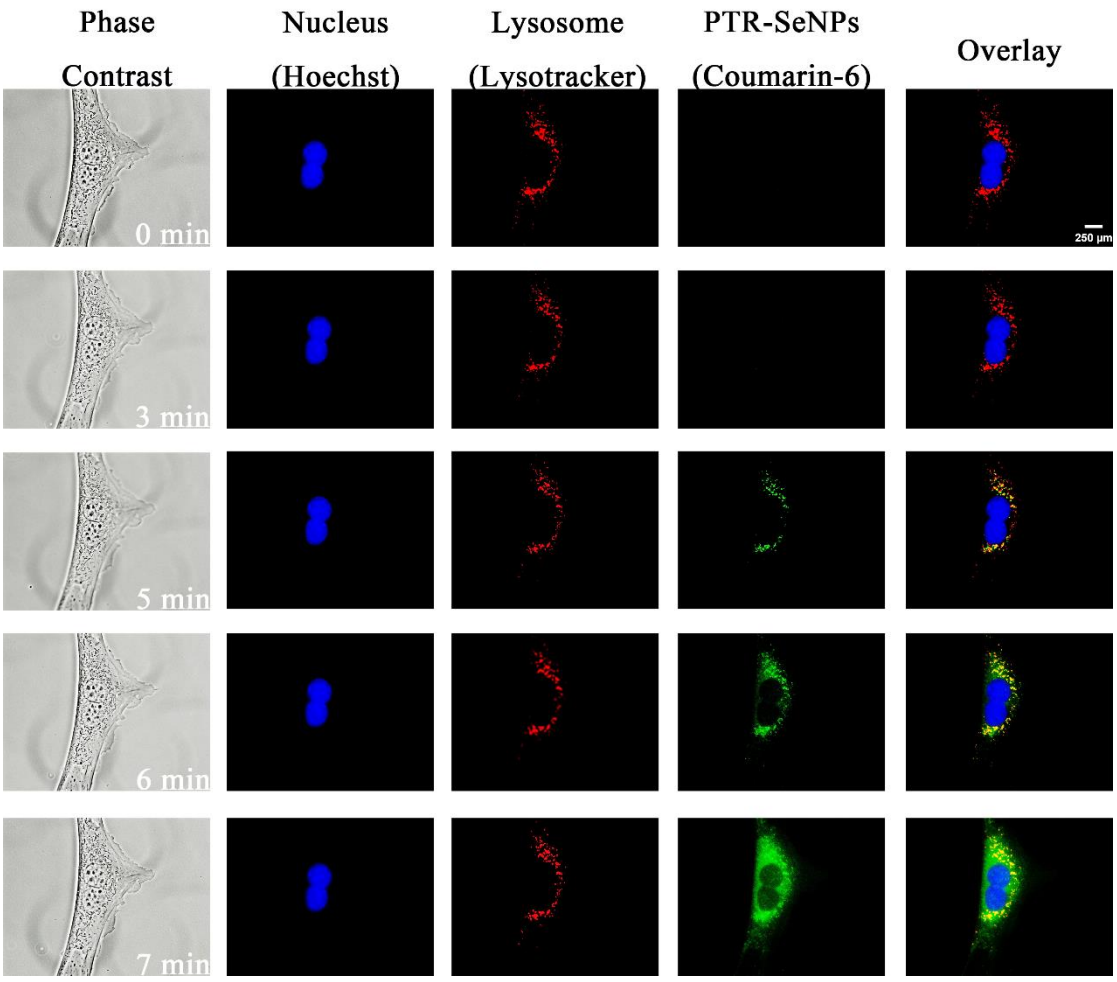

Figure 20. PTR-SeNPs co-localized with lysosomes in the MC3T3-E1 cells after cellular internalization. Cells were pre-treated with Hoechst 33342 (blue; nucleus), LysoTracker Deep Red (Red; lysosomes) and courmarin-6-loaded PTR-SeNPs (10µM; green) at 37 °C for different period of time followed by visualization under fluorescence microscope (Scale bar: 250µm).

3.7. Stimulatory Effect of PTR-SeNPs on Bone Formation Using Medaka Larvae

Japanese medaka (*Oryzias latipes*) is a teleost fish, which has been found to possess a very high similarity in bone structure and metabolism to those of mammals [91-93]. Because of having a similar estrogen profile to humans, medaka has been recently suggested to serve as a non-mammalian animal model to study sex and age-related bone metabolism *in vivo* [4]. In this study, we have successfully established a brand new *in vivo* model to investigate the simulating effect of PTR-SeNPs on bone formation using medaka larvae. By comparing the mineralization level (area and intensity of purple-red color) at different regions of vertebrae column (such as anal fin, dorsal fin and caudal fin), PTR-SeNPs (10ppm) was found to significantly enhance the vertebrate development of medaka larvae after feeding for 11 days as visualized by Alizarin Red S (bone) and Alcian Blue (cartilage) double staining (

Figure 21)

Expression of mammalian osteogenic markers such as ALP, Runx2, Osx and OPG/RANKL have been previously found in medaka fish during their bone developmental stage [94-96, 111]. Similarly, the gene expression of ALP (1.53 ± 0.1 folds), Runx2 (1.45 ± 0.10 folds), Osx (1.41 ± 0.15 folds) as well as OPG/RANKL (4.38 ± 1.31 folds) in the medaka larvae fed with PTR-SeNPs based diet (10ppm) for 2 days were all significantly up-regulated (**Figure 22**). In consistent with the findings of our *in vitro* study, PTR-SeNPs (10ppm) not only promoted osteoblastogenesis, but also indirectly inhibited osteoclastogenesis, significantly enhancing the vertebrae development in medaka fish larvae.

Control diet

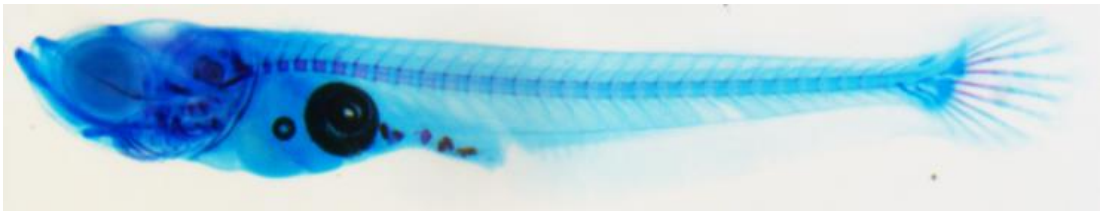

PTR-SeNPs based diet (10 ppm)

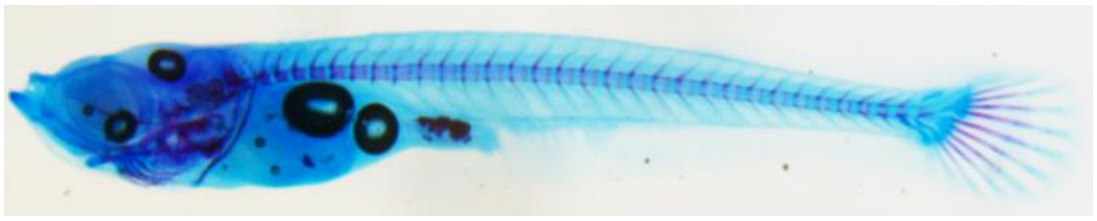

	Control diet	**PTR-SeNPs based diet (10 ppm)**
Caudal fin	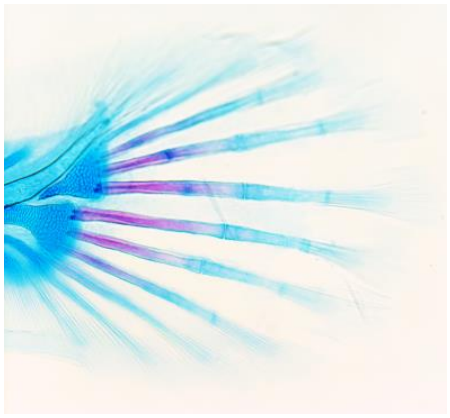	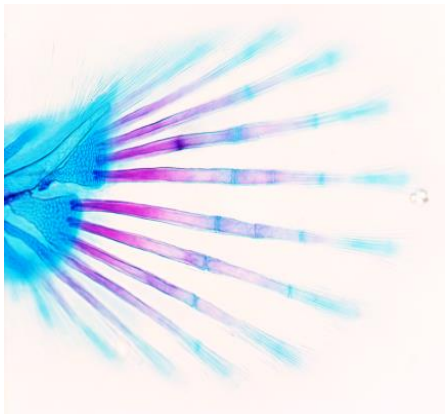
Vertebrae at caudal fin	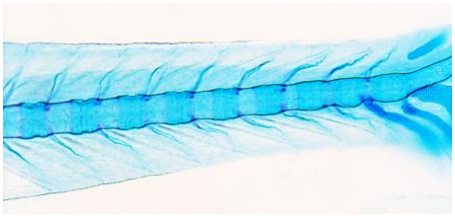	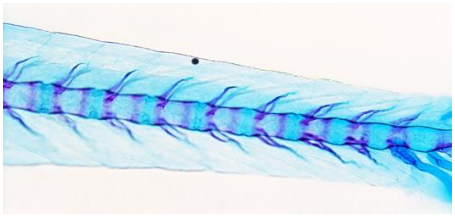
Vertebrae at dorsal	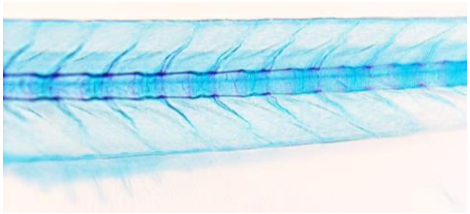	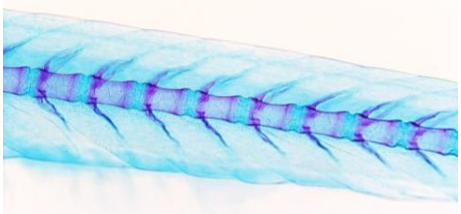
Vertebrae at anal fin	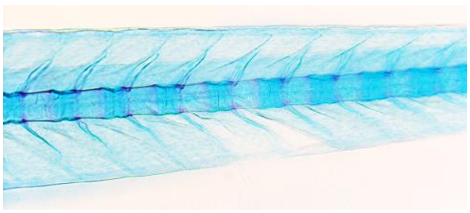	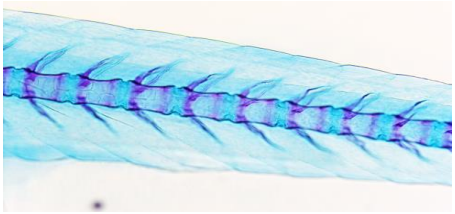

Figure 21. PTR-SeNPs enhanced the vertebrae development of medaka larvae. Medaka larvae were cultured in 6-well cell-culture plates (one medaka larvae per well) and fed either the control or PTR-SeNPs based diet (10ppm) twice daily for 11 days. Bone (pink) and cartilage (blue) were double-stained by Alizarin Red S and Alcian Blue, respectively. Images were captured by Nikon Elicpse Ci-E upright microscope.

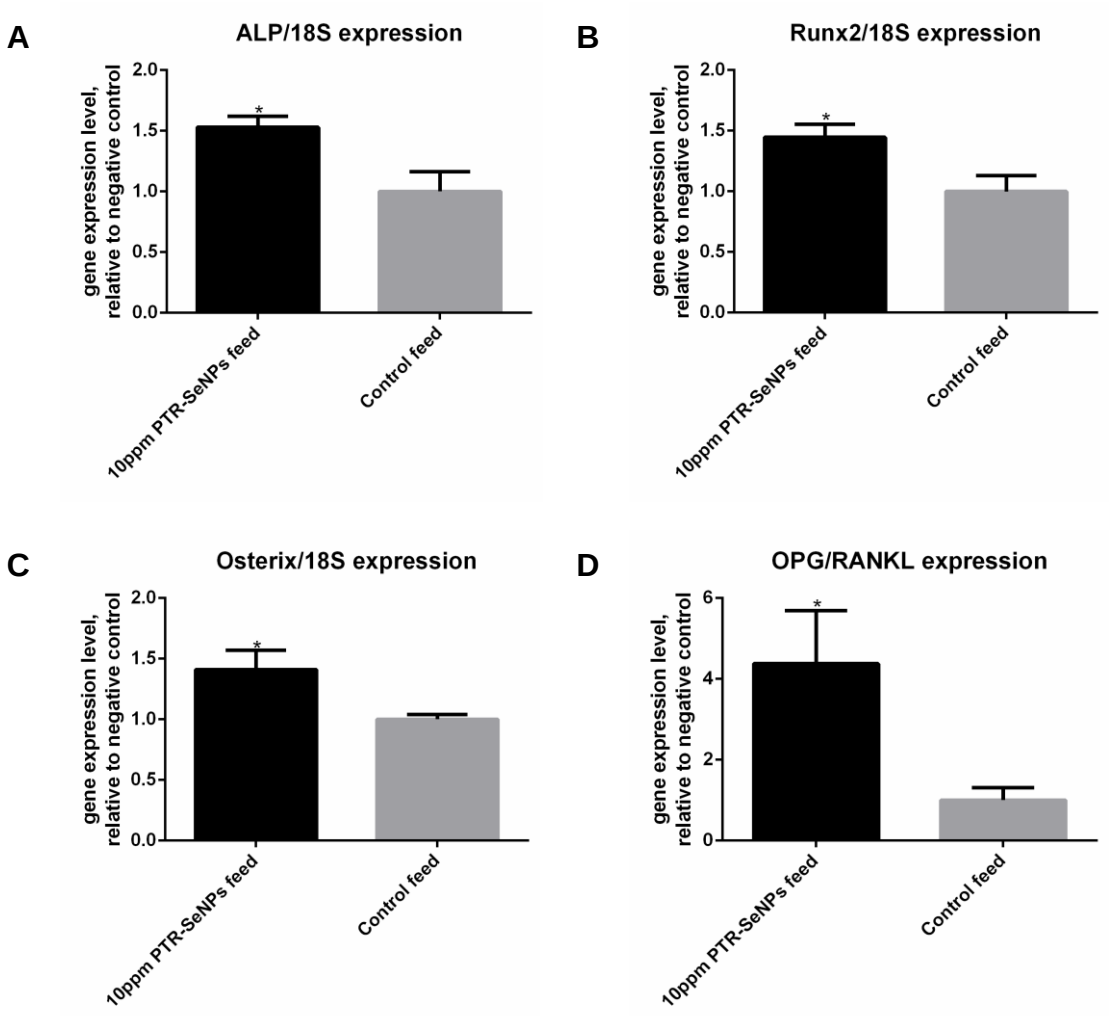

Figure 22. PTR-SeNPs upregulated the major osteogenic markers in medaka larvae during vertebrae development. Gene expression of (A) ALP, (B) Runx2, (C) Osx and (D) OPG/RANKL in medaka larvae (n = 3) fed with 10ppm of PTR-SeNPs based diet or control diet for 2 days was quantified by qPCR analysis and normalized to that of 18S. Results are mean values of three determinations ± SEM. Means with "*" are significantly different ($p < 0.05$; Student's *t* test).

3.8. Comparison between PTR-SeNPs and Other SeNPs

Table 8 briefly summarized different types of SeNPs reported in previous literatures. Interestingly, SeNPs fabricated with different stabilizers showed different physcio-chemical properties and health promoting functions. Further comparison with the osteogenic Ru@Se also indicated that PTR-SeNPs did not only possess a remarkably smaller average particle size, but also exhibited a significantly higher stability and cellular uptake efficiency (

Table 9). More importantly, in contrast to the Ru@Se, the major component of PTR-SeNPs is edible mushroom PSP instead of highly toxic and carcinogenic Ru(II) complex, suggesting its high potent to be developed as a novel agent for bone health.

Table 8. Brief summary of different types of SeNPs

Particles	Preparation method	Stabilizer	Average particles size	Effect
SeNPs fabricated with *Undarin pinnatifida* polysaccharide [78]	Redox	Polysaccharide from *Undarin pinnatifida*	59nm	Induced apoptosis of A375 human melanoma cells
SeNPs stabilized by *Pseudomonas alcapliphilia* [74]	Biosynthesis	*Pseudomonas alcaliphilia*	200nm	Unknown
Transferrin-chitosan-doxorubicin-SeNPs [112]	Redox	Transferrin Chitosan	130nm	Enhanced cellular uptake of doxorubicin and induced apoptosis of breast cancer cells
Nano-Se [113]	Redox	Bovine serum albumin	36nm	Chemoprevention via increasing glutathione-S-transferase activity
Ruthenium (II) functional SeNPs (Ru@Se) [84]	Redox	Ruthenium (II) complex	170nm	Enhanced osteoblastic differentiation in stem cell via BMP signaling pathway

Table 9. Comparison between PTR-SeNPs and Ru@Se

	PTR-SeNPs	**Ru@Se** [84]
Composition of SeNPs	PTR-PSP, Se	Ruthenium, Se
Average particles size	< 100nm	> 100nm
Stability	> 3 months (well-dispensed spherical particles in water)	Unknown; (spherical particles aggregated in water)
Safety	PTR-PSP: edible mushroom	Ru: highly toxic and carcinogenic metal
Cell line	Preosteoblasts	Stem cells
Mechanism	Via both Smad dependent and independent pathways	Via Smad dependent pathway only
Cellular uptake efficiency	5 min	48 hrs
***In vivo* study**	Medaka larvae	Unknown

3.9. Comparison between PTR-SeNPs and Other Osteogenic Nanoparticles

Table 10 briefly summarized different osteogenic nanoparticles and their possible mechanism of actions. Similar to the silica-based nanoparticles [114], PTR-SeNPs were found to enter the MC3T3-E1 cells via endocytosis followed by activating the MAPK pathways (including ERK1/2) and stimulating osteoblast differentiation and mineralization. Thus, it would be very interesting to find out whether PTR-SeNPs mediated osteoblastogenesis is related to autophagy like the silica-based nanoparticles in the MC3T3-E1 cells [114]. As proposed in Figure 23, PTR-SeNPs might enter the MC3T3-E1 cells through endocytosis followed by stimulating a MAPK pathway dependent autophagy and upregulating the expression of major osteogenic marker genes. Besides, the increased transcription of BMP-2 would further react with BMP-2 receptor to activate the BMP-2/Smad dependent pathway, hereby collectively promoting the osteoblastogenesis.

Table 10. Brief summary of different osteogenic nanoparticles

Nanoparticles	Composition	Safety	Average particles size	Cell line	Mechanism of action
Calcium phosphate nanoparticles [115]	Na_2HPO_4, $CaCl_2$, CTAB	CTAB: toxic	20nm	Bone marrow mesenchymal stem cells	Unknown
Hydroxyapatite-coated iron oxide nanoparticles[116, 117]	Fe_3O_4. Hydroxyapatite	Fe_3O_4: inedible	60nm long, 20nm wide	hFOB 1.1 human osteoblast-like cells	Enhanced fibronectin adsorption
Zinc oxide nanoparticles [118]	ZnO	Safe	30nm	Mesenchymal stem cells	Unknown
Silica-based nanoparticles [114, 119]	SiO_2	inedible	50nm	MC3T3-E1 cells	Stimulated osteoblastic differentiation and mineralization through activating the ERK1/2 pathway dependent autophagy
Gold nanoparticles [120]	Au, Sodium citrate	Safe	20nm	Mesenchymal stem cells	Promoted osteogenic differentiation via p38 pathway by causing mechanical stress

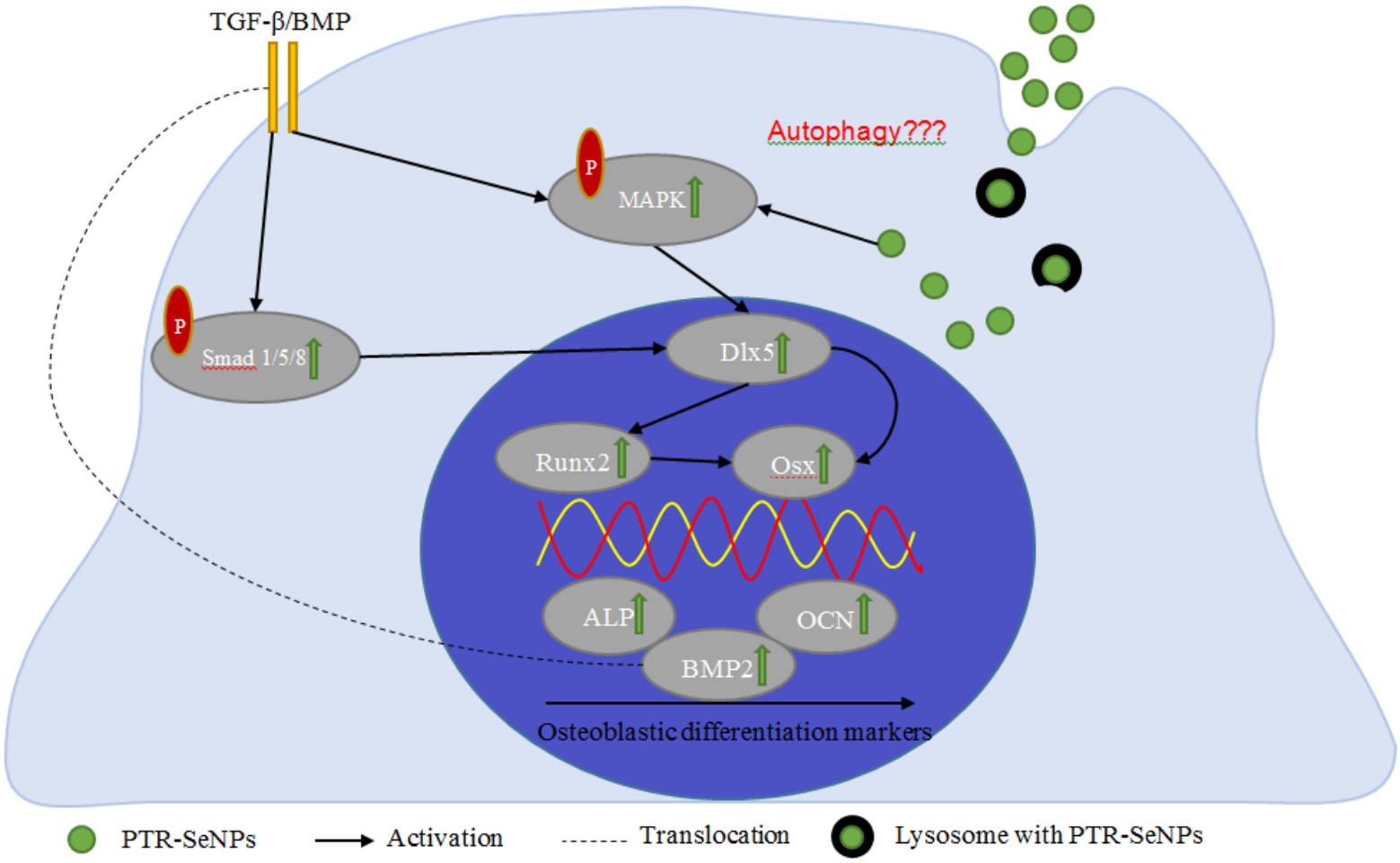

Figure 23. Possible mechanism of PTR-SeNPs stimulated osteoblastogenesis via BMP-2 signaling cascade

4. Conclusions

4.1. Conclusions

By using the mushroom polysaccharide-protein complex (PSP) isolated from *Pleurotus tuber-regium*, we have successfully prepared novel SeNPs (PTR-SeNPs) under a simple, food grade redox system. PTR-SeNPs existed as well-dispensed spherical particles in water with an average diameter of 91.3 ± 1.53 nm, possessing a polycrystalline structure with high level of Se (81.2%). X-ray Diffraction (XRD) is a versatile technique that can investigate more degree of diffraction than conventional SAED-TEM [121] and is commonly used in crystallography analysis for studying lattice structure and orientation of inorganic nano-compounds [122, 123]. Further characterization using XRD would allow providing a clearer crystal structure of the PTR-SeNPs.

Substantial previous findings have demonstrated that promoting bone formation is one of the effective strategies to prevent and/or manage postmenopausal osteoporosis. Interestingly, our study indicated that PTR-SeNPs (10μM) not only promoted osteoblastogenesis (including cell proliferation, osteogenic differentiation and bone mineral formation), but also indirectly inhibited osteoclastogenesis in the murine preosteoblast MC3T3-E1 cells mediated by both BMP-2/Smad dependent and independent pathways. Thus, it would be interesting to further characterize their direct effects on osteogenesis using different cell stages of human osteoblasts such as human

bone marrow-derived mesenchymal stem cells and hFOB 1.19 human fetal osteoblast cells.

Endocytosis has been widely reported as the major cellular uptake mechanism for nanoparticles. PTR-SeNPs (10μM) was found to co-localize with the lysosomes in the MC3T3-E1 cells as early as 5 min after cellular internalization. It is the first study of its kind to report the intracellular localization of SeNPs by MC3T3-E1 cells via endocytosis. Further elucidation of the molecular mechanism of PTR-SeNPs induced endocytosis is highly valuable.

Last but not least, we discovered that PTR-SeNPs (10ppm) could significantly enhance the vertebrate development (both bone and cartilage) of medaka larvae after feeding for 11 days together with up-regulating of those major osteogenic markers in bone metabolism. In order to develop medaka larvae as a brand new *in vivo* model for bone research, it is crucial to further determine the effect of PTR-SeNPs on the medaka fish at different life stages in terms of bone mineral density and micro-architecture using microCT as well as gene and protein levels of major osteogenic markers (both osteoblasts and osteoclasts) using qPCR and Western blotting. Besides, in order to understand the possibility of over mineralization in the PTR-SeNPs fed medaka fish,

the bone mineral density and calcification level in medaka fish at different life stages after feeding with very high concentration of PTR-SeNPs based diet (e.g. 50ppm) should be comprehensively investigated. Furthermore, verification and validation of the findings of fish model by using traditional mice or rats (mammals) are also essential.

Findings of this study could provide significant insights into the *in vitro* and *in vivo* effects of PTR-SeNPs on bone formation. Besides, medaka larvae, as a novel non-mammalian animal model for studying bone formation, could be further developed into a rapid and economical *in vivo* screening platform prior to conducting traditional animal study using mice or rats, which is relatively expensive, time-consuming, labor intensive and required plenty of space. Our long-term goal is to develop PTR-SeNPs into an evidence-based bone-forming agent for promoting the bone health of postmenopausal patients in local community.

5. References

1. Mithal, A.; Ebeling, P. Asia-Pacific Regional Audit: Epidemiology, costs and burden of osteoporosis 2013. https://www.iofbonehealth.org/sites/default/files/media/PDFs/Regional%20Audits/2013-Asia_Pacific_Audit_0_0.pdf (accessed July 13, 2017).
2. U.S. Department of Health and Human Services, O. o. t. S. G., *Bone Health and Osteoporosis: A Report of the Surgeon General*. U.S. Department of Health and Human Services, Office of the Surgeon General: Rockville, MD, U.S, 2004; Vol. 1, p 1.
3. Lau, T. W.; Leung, F.; Siu, D.; Wong, G.; Luk, K. D. K., Geriatric hip fracture clinical pathway: the Hong Kong experience. *Osteoporosis International* **2010,** *21* (Suppl 4), 627-636.
4. Shanthanagouda, A. H.; Guo, B. S.; Ye, R. R.; Chao, L.; Chiang, M. W.; Singaram, G.; Cheung, N. K.; Zhang, G.; Au, D. W., Japanese medaka: a non-mammalian vertebrate model for studying sex and age-related bone metabolism in vivo. *PLoS One* **2014,** *9* (2), e88165.
5. Cheung, E.; Bow, C.; Loong, C.; Lee, K. K.; Ho, A. Y.; Soong, C.; Chan, Y. Y.; Tan, K. C.; Kung, A. W., A secular increase in BMD in Chinese women. *Journal of Bone and Mineral Metabolism* **2014,** *32* (1), 48-55.
6. Black, D. M.; Cummings, S. R.; Karpf, D. B.; Cauley, J. A.; Thompson, D. E.; Nevitt, M. C.; Bauer, D. C.; Genant, H. K.; Haskell, W. L.; Marcus, R.; Ott, S. M.; Torner, J. C.; Quandt, S. A.; Reiss, T. F.; Ensrud, K. E., Randomised trial of effect of alendronate on risk of fracture in women with existing vertebral fractures. Fracture Intervention Trial Research Group. *Lancet* **1996,** *348* (9041), 1535-41.
7. Harris, S. T.; Watts, N. B.; Genant, H. K.; McKeever, C. D.; Hangartner, T.; Keller, M.; Chesnut, C. H.; Brown, J.; Eriksen, E. F.; Hoseyni, M. S.; Axelrod, D. W.; Miller, P. D., Effects of risedronate treatment on vertebral and nonvertebral fractures in women with postmenopausal osteoporosis: a randomized controlled trial. Vertebral Efficacy With Risedronate Therapy (VERT) Study Group. *JAMA* **1999,** *282* (14), 1344-52.
8. Abrahamsen, B.; Eiken, P.; Brixen, K., Atrial fibrillation in fracture patients treated with oral bisphosphonates. *Journal of Internal Medicine* **2009,** *265* (5), 581-92.
9. Heckbert, S. R.; Li, G.; Cummings, S. R.; Smith, N. L.; Psaty, B. M., Use of alendronate and risk of incident atrial fibrillation in women. *Archives of Internal Medicine* **2008,** *168* (8), 826-31.
10. Kim, D. H.; Rogers, J. R.; Fulchino, L. A.; Kim, C. A.; Solomon, D. H.; Kim, S. C., Bisphosphonates and risk of cardiovascular events: a meta-analysis. *PLoS One* **2015,** *10* (4), e0122646.
11. Pazianas, M.; Cooper, C.; Wang, Y.; Lange, J. L.; Russell, R. G., Atrial

fibrillation and the use of oral bisphosphonates. *Therapeutics and Clinical Risk Management* **2011,** *7*, 131-44.

12. Chesnut, C. H.; Azria, M.; Silverman, S.; Engelhardt, M.; Olson, M.; Mindeholm, L., Salmon calcitonin: a review of current and future therapeutic indications. *Osteoporosis International* **2008,** *19* (4), 479-91.
13. McClung, M. R.; Lewiecki, E. M.; Cohen, S. B.; Bolognese, M. A.; Woodson, G. C.; Moffett, A. H.; Peacock, M.; Miller, P. D.; Lederman, S. N.; Chesnut, C. H.; Lain, D.; Kivitz, A. J.; Holloway, D. L.; Zhang, C.; Peterson, M. C.; Bekker, P. J.; Group, A. B. L. S., Denosumab in postmenopausal women with low bone mineral density. *The New England Journal of Medicine* **2006,** *354* (8), 821-31.
14. McCormick, B. B.; Davis, J.; Burns, K. D., Severe Hypocalcemia Following Denosumab Injection in a Hemodialysis Patient. *American Journal of Kidney Diseases* **2012,** *60* (4), 626-628.
15. Foncubierta, A.; Gutierrez, D.; Medina, F.; Fernandez, S.; Fernandez, M. J.; Anguita, J. L., Hypersensitivity Reaction To Denosumab In Patient With Osteoporosis: Desensitization Methodology. *Journal of Allergy and Clinical Immunology* **2014,** *133* (2), AB272.
16. Delmas, P. D.; Bjarnason, N. H.; Mitlak, B. H.; Ravoux, A. C.; Shah, A. S.; Huster, W. J.; Draper, M.; Christiansen, C., Effects of raloxifene on bone mineral density, serum cholesterol concentrations, and uterine endometrium in postmenopausal women. *The New England Journal of Medicine* **1997,** *337* (23), 1641-7.
17. Kawate, H.; Takayanagi, R., Efficacy and safety of bazedoxifene for postmenopausal osteoporosis. *Clinical Interventions in Aging* **2011,** *6*, 151-60.
18. de Villiers, T. J.; Chines, A. A.; Palacios, S.; Lips, P.; Sawicki, A. Z.; Levine, A. B.; Codreanu, C.; Kelepouris, N.; Brown, J. P., Safety and tolerability of bazedoxifene in postmenopausal women with osteoporosis: results of a 5-year, randomized, placebo-controlled phase 3 trial. *Osteoporosis International* **2011,** *22* (2), 567-76.
19. Meunier, P. J.; Roux, C.; Seeman, E.; Ortolani, S.; Badurski, J. E.; Spector, T. D.; Cannata, J.; Balogh, A.; Lemmel, E. M.; Pors-Nielsen, S.; Rizzoli, R.; Genant, H. K.; Reginster, J. Y., The effects of strontium ranelate on the risk of vertebral fracture in women with postmenopausal osteoporosis. *The New England Journal of Medicine* **2004,** *350* (5), 459-68.
20. Meunier, P. J.; Slosman, D. O.; Delmas, P. D.; Sebert, J. L.; Brandi, M. L.; Albanese, C.; Lorenc, R.; Pors-Nielsen, S.; De Vernejoul, M. C.; Roces, A.; Reginster, J. Y., Strontium ranelate: dose-dependent effects in established postmenopausal vertebral osteoporosis--a 2-year randomized placebo controlled

trial. *The Journal of Clinical Endocrinology & Metabolism* **2002,** *87* (5), 2060-6.
21. Reginster, J. Y.; Felsenberg, D.; Boonen, S.; Diez-Perez, A.; Rizzoli, R.; Brandi, M. L.; Spector, T. D.; Brixen, K.; Goemaere, S.; Cormier, C.; Balogh, A.; Delmas, P. D.; Meunier, P. J., Effects of long-term strontium ranelate treatment on the risk of nonvertebral and vertebral fractures in postmenopausal osteoporosis: Results of a five-year, randomized, placebo-controlled trial. *Arthritis & Rheumatology* **2008,** *58* (6), 1687-95.
22. Dobnig, H., A review of teriparatide and its clinical efficacy in the treatment of osteoporosis. *Expert Opinion on Pharmacotherapy* **2004,** *5* (5), 1153-62.
23. Zanchetta, J. R.; Bogado, C. E.; Ferretti, J. L.; Wang, O.; Wilson, M. G.; Sato, M.; Gaich, G. A.; Dalsky, G. P.; Myers, S. L., Effects of teriparatide [recombinant human parathyroid hormone (1-34)] on cortical bone in postmenopausal women with osteoporosis. *Journal of Bone and Mineral Research* **2003,** *18* (3), 539-43.
24. Vannucci, L.; Brandi, M. L., Pharmacological management of osteoporosis - when to treat and when to stop. *Expert Review of Clinical Pharmacology* **2016**, 1-8.
25. Bjarnason, N. H.; Hassager, C.; Christiansen, C., Postmenopausal bone remodelling and hormone replacement. *Climacteric* **1998,** *1* (1), 72-9.
26. Torgerson, D. J.; Bell-Syer, S. E., Hormone replacement therapy and prevention of nonvertebral fractures: a meta-analysis of randomized trials. *JAMA* **2001,** *285* (22), 2891-7.
27. Wells, G.; Tugwell, P.; Shea, B.; Guyatt, G.; Peterson, J.; Zytaruk, N.; Robinson, V.; Henry, D.; O'Connell, D.; Cranney, A.; Group, O. M. G. a. T. O. R. A., Meta-analyses of therapies for postmenopausal osteoporosis. V. Meta-analysis of the efficacy of hormone replacement therapy in treating and preventing osteoporosis in postmenopausal women. *Endocrine Reviews* **2002,** *23* (4), 529-39.
28. Cauley, J. A.; Robbins, J.; Chen, Z.; Cummings, S. R.; Jackson, R. D.; LaCroix, A. Z.; LeBoff, M.; Lewis, C. E.; McGowan, J.; Neuner, J.; Pettinger, M.; Stefanick, M. L.; Wactawski-Wende, J.; Watts, N. B.; Investigators, W. s. H. I., Effects of estrogen plus progestin on risk of fracture and bone mineral density: the Women's Health Initiative randomized trial. *JAMA* **2003,** *290* (13), 1729-38.
29. Notelovitz, M., Estrogen therapy and osteoporosis: principles & practice. *The American journal of the medical sciences* **1997,** *313* (1), 2-12.
30. Beral, V.; Collaborators, M. W. S., Breast cancer and hormone-replacement therapy in the Million Women Study. *The Lancet* **2003,** *362* (9382), 419-427.
31. Hadjidakis, D. J.; Androulakis, I. I., Bone Remodeling. *Annals of the New York Academy of Sciences* **2006,** *1092* (1), 385-396.
32. Bernstein, J. Describe the process of bone remodeling 2014.

http://www.orthopaedicsone.com/display/Clerkship/Describe+the+process+of+bone+remodeling (accessed July 13, 2017).

33. Pittenger, M. F.; Mackay, A. M.; Beck, S. C.; Jaiswal, R. K.; Douglas, R.; Mosca, J. D.; Moorman, M. A.; Simonetti, D. W.; Craig, S.; Marshak, D. R., Multilineage potential of adult human mesenchymal stem cells. *Science* **1999,** *284* (5411), 143-147.
34. Huang, W.; Yang, S.; Shao, J.; Li, Y.-P., Signaling and transcriptional regulation in osteoblast commitment and differentiation. *Frontiers in bioscience: a journal and virtual library* **2007,** *12*, 3068.
35. Sharili, A.-S.; Allen, S.; Smith, K.; Hargreaves, J.; Price, J.; McGonnell, I., Expression of Snail2 in long bone osteosarcomas correlates with tumour malignancy. *Tumor Biology* **2011,** *32* (3), 515-526.
36. Canalis, E.; Economides, A. N.; Gazzerro, E., Bone morphogenetic proteins, their antagonists, and the skeleton. *Endocrine Reviews* **2003,** *24* (2), 218-35.
37. Chen, D.; Zhao, M.; Mundy, G. R., Bone morphogenetic proteins. *Growth Factors* **2004,** *22* (4), 233-41.
38. Cao, X.; Chen, D., The BMP signaling and in vivo bone formation. *Gene* **2005,** *357* (1), 1-8.
39. Anderson, H. C.; Hodges, P. T.; Aguilera, X. M.; Missana, L.; Moylan, P. E., Bone morphogenetic protein (BMP) localization in developing human and rat growth plate, metaphysis, epiphysis, and articular cartilage. *Journal of Histochemistry and Cytochemistry* **2000,** *48* (11), 1493-502.
40. Daluiski, A.; Engstrand, T.; Bahamonde, M. E.; Gamer, L. W.; Agius, E.; Stevenson, S. L.; Cox, K.; Rosen, V.; Lyons, K. M., Bone morphogenetic protein-3 is a negative regulator of bone density. *Nature Genetics* **2001,** *27* (1), 84-8.
41. Derynck, R.; Akhurst, R. J.; Balmain, A., TGF-beta signaling in tumor suppression and cancer progression. *Nature Genetics* **2001,** *29* (2), 117-29.
42. Massagué, J., How cells read TGF-beta signals. *Nature Reviews Molecular Cell Biology* **2000,** *1* (3), 169-78.
43. Zhang, Y. W.; Yasui, N.; Ito, K.; Huang, G.; Fujii, M.; Hanai, J.; Nogami, H.; Ochi, T.; Miyazono, K.; Ito, Y., A RUNX2/PEBP2alpha A/CBFA1 mutation displaying impaired transactivation and Smad interaction in cleidocranial dysplasia. *Proceedings of the National Academy of Sciences* **2000,** *97* (19), 10549-54.
44. Miyazono, K.; Maeda, S.; Imamura, T., Coordinate regulation of cell growth and differentiation by TGF-beta superfamily and Runx proteins. *Oncogene* **2004,** *23* (24), 4232-7.
45. Ito, Y.; Miyazono, K., RUNX transcription factors as key targets of TGF-beta

superfamily signaling. *Current Opinion in Genetics & Development* **2003,** *13* (1), 43-7.

46. Miyama, K.; Yamada, G.; Yamamoto, T. S.; Takagi, C.; Miyado, K.; Sakai, M.; Ueno, N.; Shibuya, H., A BMP-inducible gene, dlx5, regulates osteoblast differentiation and mesoderm induction. *Developmental Biology* **1999,** *208* (1), 123-33.
47. Lee, M. H.; Kim, Y. J.; Kim, H. J.; Park, H. D.; Kang, A. R.; Kyung, H. M.; Sung, J. H.; Wozney, J. M.; Ryoo, H. M., BMP-2-induced Runx2 expression is mediated by Dlx5, and TGF-beta 1 opposes the BMP-2-induced osteoblast differentiation by suppression of Dlx5 expression. *Journal of Biological Chemistry* **2003,** *278* (36), 34387-94.
48. de Jong, D. S.; Vaes, B. L.; Dechering, K. J.; Feijen, A.; Hendriks, J. M.; Wehrens, R.; Mummery, C. L.; van Zoelen, E. J.; Olijve, W.; Steegenga, W. T., Identification of novel regulators associated with early-phase osteoblast differentiation. *Journal of Bone and Mineral Research* **2004,** *19* (6), 947-58.
49. Korchynskyi, O.; Dechering, K. J.; Sijbers, A. M.; Olijve, W.; ten Dijke, P., Gene array analysis of bone morphogenetic protein type I receptor-induced osteoblast differentiation. *Journal of Bone and Mineral Research* **2003,** *18* (7), 1177-85.
50. Guicheux, J.; Lemonnier, J.; Ghayor, C.; Suzuki, A.; Palmer, G.; Caverzasio, J., Activation of p38 mitogen-activated protein kinase and c-Jun-NH2-terminal kinase by BMP-2 and their implication in the stimulation of osteoblastic cell differentiation. *Journal of Bone and Mineral Research* **2003,** *18* (11), 2060-8.
51. Lai, C. F.; Cheng, S. L., Signal transductions induced by bone morphogenetic protein-2 and transforming growth factor-beta in normal human osteoblastic cells. *Journal of Biological Chemistry* **2002,** *277* (18), 15514-22.
52. Lemonnier, J.; Ghayor, C.; Guicheux, J.; Caverzasio, J., Protein kinase C-independent activation of protein kinase D is involved in BMP-2-induced activation of stress mitogen-activated protein kinases JNK and p38 and osteoblastic cell differentiation. *Journal of Biological Chemistry* **2004,** *279* (1), 259-64.
53. Lee, K. S.; Hong, S. H.; Bae, S. C., Both the Smad and p38 MAPK pathways play a crucial role in Runx2 expression following induction by transforming growth factor-beta and bone morphogenetic protein. *Oncogene* **2002,** *21* (47), 7156-63.
54. Lee, K. S.; Kim, H. J.; Li, Q. L.; Chi, X. Z.; Ueta, C.; Komori, T.; Wozney, J. M.; Kim, E. G.; Choi, J. Y.; Ryoo, H. M.; Bae, S. C., Runx2 is a common target of transforming growth factor beta1 and bone morphogenetic protein 2, and cooperation between Runx2 and Smad5 induces osteoblast-specific gene

expression in the pluripotent mesenchymal precursor cell line C2C12. *Molecular and Cellular Biology* **2000,** *20* (23), 8783-92.

55. Lee, M. H.; Javed, A.; Kim, H. J.; Shin, H. I.; Gutierrez, S.; Choi, J. Y.; Rosen, V.; Stein, J. L.; van Wijnen, A. J.; Stein, G. S.; Lian, J. B.; Ryoo, H. M., Transient upregulation of CBFA1 in response to bone morphogenetic protein-2 and transforming growth factor beta1 in C2C12 myogenic cells coincides with suppression of the myogenic phenotype but is not sufficient for osteoblast differentiation. *Journal of Cellular Biochemistry* **1999,** *73* (1), 114-25.
56. Nakashima, K.; Zhou, X.; Kunkel, G.; Zhang, Z.; Deng, J. M.; Behringer, R. R.; de Crombrugghe, B., The novel zinc finger-containing transcription factor osterix is required for osteoblast differentiation and bone formation. *Cell* **2002,** *108* (1), 17-29.
57. Yagi, K.; Tsuji, K.; Nifuji, A.; Shinomiya, K.; Nakashima, K.; DeCrombrugghe, B.; Noda, M., Bone morphogenetic protein-2 enhances osterix gene expression in chondrocytes. *Journal of Cellular Biochemistry* **2003,** *88* (6), 1077-83.
58. Lee, M. H.; Kwon, T. G.; Park, H. S.; Wozney, J. M.; Ryoo, H. M., BMP-2-induced Osterix expression is mediated by Dlx5 but is independent of Runx2. *Biochemical and Biophysical Research Communications* **2003,** *309* (3), 689-94.
59. Celil, A. B.; Hollinger, J. O.; Campbell, P. G., Osx transcriptional regulation is mediated by additional pathways to BMP2/Smad signaling. *Journal of Cellular Biochemistry* **2005,** *95* (3), 518-28.
60. Wu, M.; Chen, G.; Li, Y. P., TGF-β and BMP signaling in osteoblast, skeletal development, and bone formation, homeostasis and disease. *Bone Research* **2016,** *4*, 16009.
61. Shore, E. M.; Kaplan, F. S., Inherited human diseases of heterotopic bone formation. *Nature Reviews Rheumatology* **2010,** *6* (9), 518-27.
62. Monsen, E. R., Dietary Reference Intakes for The Antioxidant Nutrients. *Journal of the American Dietetic Association* **2000,** *100* (6), 637-640.
63. Davis, C. D.; Tsuji, P. A.; Milner, J. A., Selenoproteins and Cancer Prevention. *Annu. Rev. Nutr.* **2012,** *32* (1), 73-95.
64. Cao, J. J.; Gregoire, B. R.; Zeng, H., Selenium Deficiency Decreases Antioxidative Capacity and Is Detrimental to Bone Microarchitecture in Mice. *The Journal of Nutrition* **2012,** *142* (8), 1526-1531.
65. Saito, Y.; Yoshida, Y.; Akazawa, T.; Takahashi, K.; Niki, E., Cell Death Caused by Selenium Deficiency and Protective Effect of Antioxidants. *Journal of Biological Chemistry* **2003,** *278* (41), 39428-39434.
66. Zhang, J.; Munger, R. G.; West, N. A.; Cutler, D. R.; Wengreen, H. J.; Corcoran,

C. D., Antioxidant Intake and Risk of Osteoporotic Hip Fracture in Utah: An Effect Modified by Smoking Status. *American Journal of Epidemiology* **2006,** *163* (1), 9-17.

67. Moreno-Reyes, R.; Egrise, D.; Nève, J.; Pasteels, J.-L.; Schoutens, A., Selenium Deficiency-Induced Growth Retardation Is Associated with an Impaired Bone Metabolism and Osteopenia. *Journal of Bone and Mineral Research* **2001,** *16* (8), 1556-1563.
68. Moreno-Reyes, R.; Mathieu, F.; Boelaert, M.; Begaux, F.; Suetens, C.; Rivera, M. T.; Nève, J.; Perlmutter, N.; Vanderpas, J., Selenium and iodine supplementation of rural Tibetan children affected by Kashin-Beck osteoarthropathy. *The American Journal of Clinical Nutrition* **2003,** *78* (1), 137-144.
69. Liu, H.; Bian, W.; Liu, S.; Huang, K., Selenium protects bone marrow stromal cells against hydrogen peroxide-induced inhibition of osteoblastic differentiation by suppressing oxidative stress and ERK signaling pathway. *Biological Trace Element Research* **2012,** *150* (1-3), 441-50.
70. Wang, H.; Zhang, J.; Yu, H., Elemental selenium at nano size possesses lower toxicity without compromising the fundamental effect on selenoenzymes: comparison with selenomethionine in mice. *Free Radical Biology & Medicine* **2007,** *42* (10), 1524-33.
71. Yang, F.; Tang, Q.; Zhong, X.; Bai, Y.; Chen, T.; Zhang, Y.; Li, Y.; Zheng, W., Surface decoration by Spirulina polysaccharide enhances the cellular uptake and anticancer efficacy of selenium nanoparticles. *International Journal of Nanomedicine* **2012,** *7*, 835-844.
72. Benko, I.; Nagy, G.; Tanczos, B.; Ungvari, E.; Sztrik, A.; Eszenyi, P.; Prokisch, J.; Banfalvi, G., Subacute toxicity of nano-selenium compared to other selenium species in mice. *Environmental toxicology and chemistry* **2012,** *31* (12), 2812-2820.
73. Zhang, J.; Wang, H.; Yan, X.; Zhang, L., Comparison of short-term toxicity between Nano-Se and selenite in mice. *Life Sciences* **2005,** *76* (10), 1099-109.
74. Zhang, W.; Chen, Z.; Liu, H.; Zhang, L.; Gao, P.; Li, D., Biosynthesis and structural characteristics of selenium nanoparticles by Pseudomonas alcaliphila. *Colloids and Surfaces B: Biointerfaces* **2011,** *88* (1), 196-201.
75. Zhang, Y.; Wang, J.; Zhang, L., Creation of highly stable selenium nanoparticles capped with hyperbranched polysaccharide in water. *Langmuir* **2010,** *26* (22), 17617-17623.
76. Kong, L.; Yuan, Q.; Zhu, H.; Li, Y.; Guo, Q.; Wang, Q.; Bi, X.; Gao, X., The suppression of prostate LNCaP cancer cells growth by Selenium nanoparticles through Akt/Mdm2/AR controlled apoptosis. *Biomaterials* **2011,** *32* (27),

6515-6522.

77. Wu, H.; Zhu, H.; Li, X.; Liu, Z.; Zheng, W.; Chen, T.; Yu, B.; Wong, K.-H., Induction of Apoptosis and Cell Cycle Arrest in A549 Human Lung Adenocarcinoma Cells by Surface-Capping Selenium Nanoparticles: An Effect Enhanced by Polysaccharide–Protein Complexes from Polyporus rhinocerus. *J. Agric. Food Chem.* **2013,** *61* (41), 9859-9866.
78. Chen, T.; Wong, Y. S.; Zheng, W.; Bai, Y.; Huang, L., Selenium nanoparticles fabricated in Undaria pinnatifida polysaccharide solutions induce mitochondria-mediated apoptosis in A375 human melanoma cells. *Colloids and Surfaces B: Biointerfaces* **2008,** *67* (1), 26-31.
79. Huang, N.; Guo, M.; Huang, L., Tiger milk mushroom (Pleurotus tuber-regium (Fr.) Sing.) and its cultivation. *Edible Fungi China* **1996,** *16*, 13-14.
80. Zadrazil, F., Pleurotus (Lentinus) tuber-regium. *Mushroom Information* **1996,** *109*, 24-29.
81. Wong, K.-H.; Cheung, P. C. K., Sclerotium of Culinary-Medicinal King Tuber Oyster Mushroom, Pleurotus tuberregium (Fr.) Singer (Agaricomycetideae): Its Cultivation, Biochemical Composition, and Biopharmacological Effects (Review). *International Journal of Medicinal Mushrooms* **2008,** *10* (4).
82. Wu, H.; Li, X.; Liu, W.; Chen, T.; Li, Y.; Zheng, W.; Man, C. W.-Y.; Wong, M.-K.; Wong, K.-H., Surface decoration of selenium nanoparticles by mushroom polysaccharides-protein complexes to achieve enhanced cellular uptake and antiproliferative activity. *Journal of Materials Chemistry* **2012,** *22* (19), 9602-9610.
83. Cheung, W. M.; Ng, W. W.; Kung, A. W., Dimethyl sulfoxide as an inducer of differentiation in preosteoblast MC3T3-E1 cells. *FEBS Letters* **2006,** *580* (1), 121-6.
84. Zheng, C.; Wang, J.; Liu, Y.; Yu, Q.; Liu, Y.; Deng, N.; Liu, J., Functional Selenium Nanoparticles Enhanced Stem Cell Osteoblastic Differentiation through BMP Signaling Pathways

Advanced Functional Materials Volume 24, Issue 43. *Advanced Functional Materials* **2014,** *24* (43), 6872-6883.

85. Ekkapongpisit, M.; Giovia, A.; Follo, C.; Caputo, G.; Isidoro, C., Biocompatibility, endocytosis, and intracellular trafficking of mesoporous silica and polystyrene nanoparticles in ovarian cancer cells: effects of size and surface charge groups. *International Journal of Nanomedicine* **2012,** *7*, 4147-4158.
86. Deyhim, F.; Stoecker, B. J.; Brusewitz, G. H.; Arjmandi, B. H., The effects of estrogen depletion and isoflavones on bone metabolism in rats. *Nutrition Research* **2003,** *23* (1), 123-130.

87. Ducy, P.; Desbois, C.; Boyce, B.; Pinero, G.; Story, B.; Dunstan, C.; Smith, E.; Bonadio, J.; Goldstein, S.; Gundberg, C.; Bradley, A.; Karsenty, G., Increased bone formation in osteocalcin-deficient mice. *Nature* **1996,** *382* (6590), 448-52.
88. Westerlind, K. C.; Wakley, G. K.; Evans, G. L.; Turner, R. T., Estrogen does not increase bone formation in growing rats. *Endocrinology* **1993,** *133* (6), 2924-34.
89. Chen, J.; Long, F., β-catenin promotes bone formation and suppresses bone resorption in postnatal growing mice. *Journal of Bone and Mineral Research* **2013,** *28* (5), 1160-9.
90. Renn, J.; Winkler, C.; Schartl, M.; Fischer, R.; Goerlich, R., Zebrafish and medaka as models for bone research including implications regarding space-related issues. *Protoplasma* **2006,** *229* (2-4), 209-14.
91. Ekanayake, S.; Hall, B. K., The development of acellularity of the vertebral bone of the Japanese medaka, Oryzias latipes (Teleostei; Cyprinidontidae). *Journal of Morphology* **1987,** *193* (3), 253-61.
92. Langille, R. M.; Hall, B. K., Development of the head skeleton of the Japanese medaka, Oryzias latipes (Teleostei). *Journal of Morphology* **1987,** *193* (2), 135-158.
93. Nemoto, Y.; Higuchi, K.; Baba, O.; Kudo, A.; Takano, Y., Multinucleate osteoclasts in medaka as evidence of active bone remodeling. *Bone* **2007,** *40* (2), 399-408.
94. Renn, J.; Büttner, A.; To, T. T.; Chan, S. J.; Winkler, C., A col10a1:nlGFP transgenic line displays putative osteoblast precursors at the medaka notochordal sheath prior to mineralization. *Developmental Biology* **2013,** *381* (1), 134-43.
95. Renn, J.; Winkler, C., Osterix/Sp7 regulates biomineralization of otoliths and bone in medaka (Oryzias latipes). *Matrix Biology* **2014,** *34*, 193-204.
96. Yasutake, J.; Inohaya, K.; Kudo, A., Twist functions in vertebral column formation in medaka, Oryzias latipes. *Mechanisms of Development* **2004,** *121* (7-8), 883-94.
97. Groot, P. A. d., Selenium. In *Handbook of Stable Isotope Analytical Techniques*, Groot, P. A. d., Ed. Elsevier: Amsterdam, 2009; Vol. 2, pp 723-739.
98. Egerton, R. F., an introduction to TEM, SEM, and AEM. In *Physical principles of electron microscopy*, 1 ed.; Springer Science & Business Media: U.S., 2005; p 210.
99. Horikoshi, S.; Serpone, N., Introduction to Nanoparticles. In *Microwaves in Nanoparticle Synthesis*, Satoshi Horikoshi, N. S., Ed. Wiley-VCH Verlag GmbH & Co. KGaA: 2013; pp 1-24.
100. Filipe, V.; Hawe, A.; Jiskoot, W., Critical Evaluation of Nanoparticle Tracking Analysis (NTA) by NanoSight for the Measurement of Nanoparticles and Protein

Aggregates. *Pharmaceutical Research* **2010,** *27* (5), 796-810.
101. Merkus, H. G., *Particle size measurements: fundamentals, practice, quality*. Springer Science & Business Media: 2009; Vol. 17.
102. Mary, K. A.; Unnikrishnan, N.; Philip, R., Cubic to amorphous transformation of Se in silica with improved ultrafast optical nonlinearity. *RSC Advances* **2015,** *5* (18), 14034-14041.
103. Vekariya, K. K.; Kaur, J.; Tikoo, K., Alleviating anastrozole induced bone toxicity by selenium nanoparticles in SD rats. *Toxicology and Applied Pharmacology* **2013,** *268* (2), 212-20.
104. Franceschi, R. T.; Xiao, G., Regulation of the osteoblast-specific transcription factor, Runx2 Responsiveness to multiple signal transduction pathways. *Journal of Cellular Biochemistry* **2003,** *88* (3), 446-454.
105. Komori, T., Regulation of osteoblast differentiation by transcription factors. *Journal of Cellular Biochemistry* **2006,** *99* (5), 1233-1239.
106. Ducy, P.; Zhang, R.; Geoffroy, V.; Ridall, A. L.; Karsenty, G., Osf2/Cbfa1: a transcriptional activator of osteoblast differentiation. *Cell* **1997,** *89* (5), 747-54.
107. Komori, T.; Yagi, H.; Nomura, S.; Yamaguchi, A.; Sasaki, K.; Deguchi, K.; Shimizu, Y.; Bronson, R. T.; Gao, Y. H.; Inada, M.; Sato, M.; Okamoto, R.; Kitamura, Y.; Yoshiki, S.; Kishimoto, T., Targeted disruption of Cbfa1 results in a complete lack of bone formation owing to maturational arrest of osteoblasts. *Cell* **1997,** *89* (5), 755-64.
108. Otto, F.; Thornell, A. P.; Crompton, T.; Denzel, A.; Gilmour, K. C.; Rosewell, I. R.; Stamp, G. W.; Beddington, R. S.; Mundlos, S.; Olsen, B. R.; Selby, P. B.; Owen, M. J., Cbfa1, a candidate gene for cleidocranial dysplasia syndrome, is essential for osteoblast differentiation and bone development. *Cell* **1997,** *89* (5), 765-71.
109. Hofbauer, L.; Kuhne, C.; Viereck, V., The OPG/RANKL/RANK system in metabolic bone diseases. *Journal of Musculoskeletal and Neuronal Interactions* **2004,** *4* (3), 268.
110. Khosla, S., Minireview: The opg/rankl/rank system. *Endocrinology* **2001,** *142* (12), 5050-5055.
111. Inohaya, K.; Kudo, A., Temporal and spatial patterns of cbfal expression during embryonic development in the teleost, Oryzias latipes. *Development Genes and Evolution* **2000,** *210* (11), 570-4.
112. Huang, Y.; He, L.; Liu, W.; Fan, C.; Zheng, W.; Wong, Y. S.; Chen, T., Selective cellular uptake and induction of apoptosis of cancer-targeted selenium nanoparticles. *Biomaterials* **2013,** *34* (29), 7106-16.
113. Peng, D.; Zhang, J.; Liu, Q.; Taylor, E. W., Size effect of elemental selenium nanoparticles (Nano-Se) at supranutritional levels on selenium accumulation and

glutathione S-transferase activity. *Journal of Inorganic Biochemistry* **2007,** *101* (10), 1457-63.

114. Ha, S. W.; Weitzmann, M. N.; Beck, G. R., Bioactive silica nanoparticles promote osteoblast differentiation through stimulation of autophagy and direct association with LC3 and p62. *ACS Nano* **2014,** *8* (6), 5898-910.
115. Hu, Q.; Tan, Z.; Liu, Y.; Tao, J.; Cai, Y.; Zhang, M.; Pan, H.; Xu, X.; Tang, R., Effect of crystallinity of calcium phosphate nanoparticles on adhesion, proliferation, and differentiation of bone marrow mesenchymal stem cells. *Journal of Materials Chemistry* **2007,** *17* (44), 4690-4698.
116. Tran, N.; Hall, D.; Webster, T. J., Mechanisms of enhanced osteoblast gene expression in the presence of hydroxyapatite coated iron oxide magnetic nanoparticles. *Nanotechnology* **2012,** *23* (45), 455104.
117. Tran, N.; Webster, T. J., Increased osteoblast functions in the presence of hydroxyapatite-coated iron oxide nanoparticles. *Acta Biomaterialia* **2011,** *7* (3), 1298-306.
118. Foroutan, T.; mousavi, s., The effects of zinc oxide nanoparticles on differentiation of human mesenchymal stem cells to osteoblast. *Nanomedicine Journal* **2014,** *1* (5), 308-314.
119. Beck, G. R.; Ha, S. W.; Camalier, C. E.; Yamaguchi, M.; Li, Y.; Lee, J. K.; Weitzmann, M. N., Bioactive silica-based nanoparticles stimulate bone-forming osteoblasts, suppress bone-resorbing osteoclasts, and enhance bone mineral density in vivo. *Nanomedicine* **2012,** *8* (6), 793-803.
120. Yi, C.; Liu, D.; Fong, C. C.; Zhang, J.; Yang, M., Gold nanoparticles promote osteogenic differentiation of mesenchymal stem cells through p38 MAPK pathway. *ACS Nano* **2010,** *4* (11), 6439-48.
121. Chung, F. H., Quantitative interpretation of X-ray diffraction patterns of mixtures. II. Adiabatic principle of X-ray diffraction analysis of mixtures. *Journal of Applied Crystallography* **1974,** *7* (6), 526-531.
122. Zhang, S.-Y.; Zhang, J.; Wang, H.-Y.; Chen, H.-Y., Synthesis of selenium nanoparticles in the presence of polysaccharides. *Materials Letters* **2004,** *58* (21), 2590-2594.
123. Shin, Y.; Blackwood, J. M.; Bae, I.-T.; Arey, B. W.; Exarhos, G. J., Synthesis and stabilization of selenium nanoparticles on cellulose nanocrystal. *Materials Letters* **2007,** *61* (21), 4297-4300.